



# Synthesis, characterization, photophysics and electrophosphorescent applications of phosphorescent platinum cyclometalated complexes with 9-arylcarbazole moieties

Cheuk-Lam Ho<sup>a,\*</sup>, Wai-Yeung Wong<sup>a,\*</sup>, Bing Yao<sup>b</sup>, Zhiyuen Xie<sup>b,\*</sup>, Lixiang Wang<sup>b</sup>, Zhenyang Lin<sup>c</sup>

<sup>a</sup> Department of Chemistry and Centre for Advanced Luminescence Materials, Hong Kong Baptist University, Waterloo Road, Kowloon Tong, Hong Kong, PR China

<sup>b</sup> State Key Laboratory of Polymer Physics and Chemistry, Changchun Institute of Applied Chemistry, Chinese Academy of Sciences, Changchun 130022, PR China

<sup>c</sup> Department of Chemistry, The Hong Kong University of Science and Technology, Clearwater Bay, Hong Kong, PR China

## ARTICLE INFO

### Article history:

Received 5 February 2009

Received in revised form 27 February 2009

Accepted 2 March 2009

Available online 9 March 2009

### Keywords:

Carbazole

Platinum complexes

Optical properties

Organic light-emitting diodes

Phosphorescence

## ABSTRACT

A series of cyclometalating platinum(II) complexes with substituted 9-arylcarbazolyl chromophores have been synthesized and characterized. These complexes are thermally stable and most of them have been characterized by X-ray crystallography. The phosphorescence emissions of the complexes are dominated by <sup>3</sup>MLCT excited states. The excited state properties of these complexes can be modulated by varying the electronic characteristics of the cyclometalating ligands via substituent effects, thus allowing the emission to be tuned from bright green to yellow, orange and red light. The correlation between the functional properties of these metallophosphors and the results of density functional theory calculations was made. Because of the propensity of the electron-rich carbazolyl group to facilitate hole injection/transport, the presence of such moiety can increase the highest occupied molecular orbital levels and improve the charge balance in the resulting complexes relative to the parent platinum(II) phosphor with 2-phenylpyridine ligand. The solution-processed electrophosphorescent organic light-emitting diodes doped with these platinum-based phosphors have been fabricated which showed a maximum external quantum efficiency of 2.77% for the best device, corresponding to a power efficiency of 3.48 lm/W and a luminance efficiency of 8.49 cd/A. The present work enables the rational design of platinum-carbazolyl electrophosphors by synthetically tailoring the structure of carbazolylpyridine ring that can permit good color-tuning versatility suitable for multi-color display technology.

© 2009 Elsevier B.V. All rights reserved.

## 1. Introduction

Luminescent platinum(II) compounds with organic conjugated ligands have attracted much attention since they may potentially be used as new materials for applications, including organic light-emitting devices (OLEDs) [1,2], dye-sensitized solar cells [3], photoreceptors in biological molecules [4], etc. In particular, research on OLEDs has made significant advances by many research groups over the past several years, demonstrating them as candidates for full-color display applications. For OLED applications, successful materials used should be facile with balanced charge transport as well as high conversion efficiency of excitons to light [5]. Although relatively fewer d<sup>8</sup> metal complexes are known to be emissive in fluid solutions at room temperature compared to other metal complexes, the phosphorescence of cyclometalated platinum(II) complexes has been well documented. The heavy Pt(II)

metal ion results in strong spin-orbit coupling in these complexes, which promotes efficient mixing of singlet and triplet states, thus enhancing phosphorescence emission and shortening emission lifetimes [6,7]. Room temperature phosphorescence emission from simple Pt(II) acetylides is rarely detected due to the presence of low-lying metal-centered excited states, which provide facile radiationless deactivation pathways via molecular distortion [8–10]. Thus, in order to obtain strong luminescence at room temperature it is necessary to utilize ligands with low-lying excited state orbitals or strong electron-donating ability. The strong ligand field associated with such ligands raises the energy of the metal *d*–*d* states, withdrawing their deactivating effect. Among them, Pt(II) complexes incorporating pyridine ligands such as bipyridine [11–23] and terpyridine [24] derivatives have attracted a great deal of interest as luminescent dyes for OLED applications since they often exhibit high phosphorescence quantum yields. On the other hand, several cyclometalated homo- or heteroleptic Pt(II) complexes based on 2-phenylpyridine (ppy) and analogues have been reported in the literature [25–27].

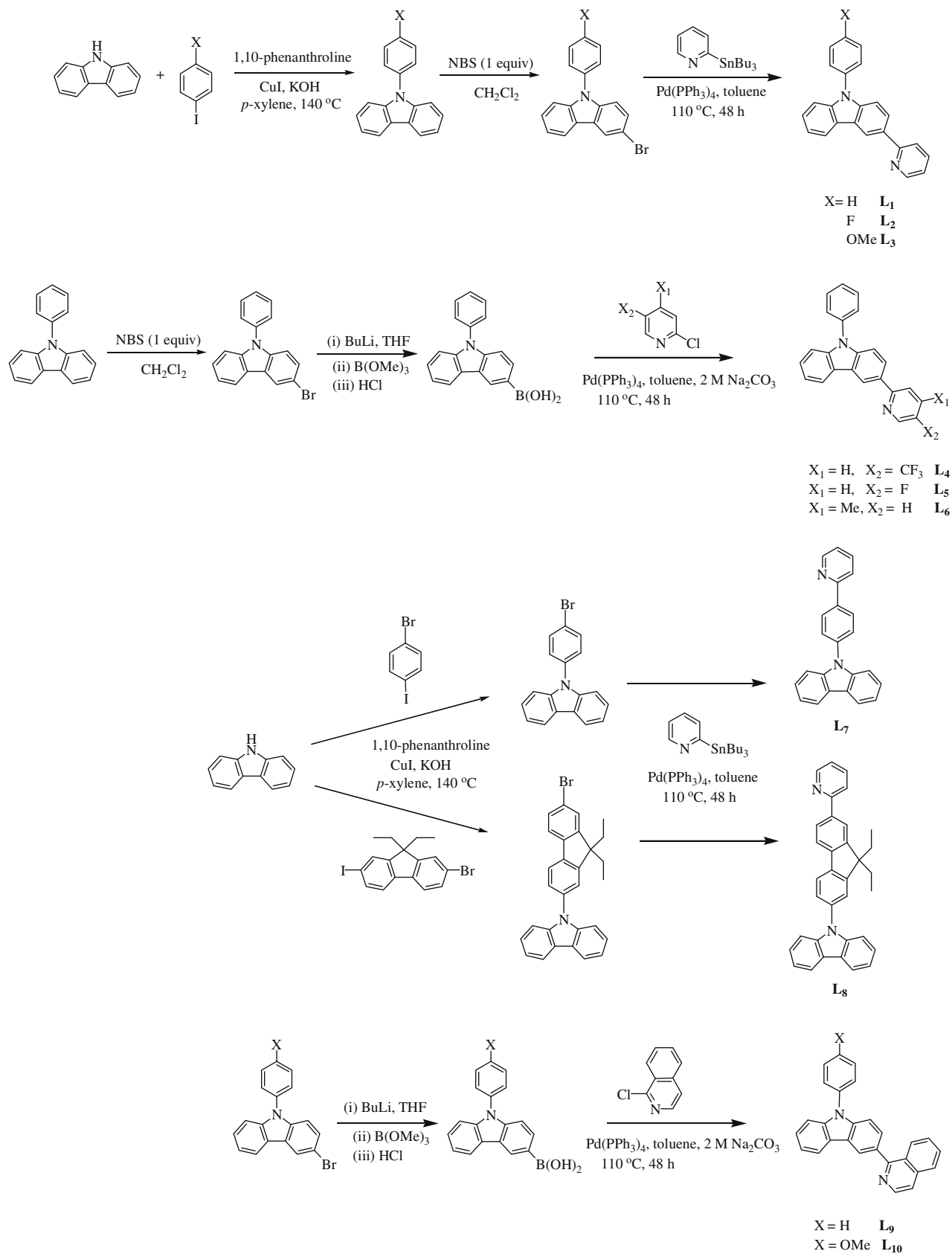
In order to better meet the requirements of OLEDs, a proper choice of the electron and hole-transport materials is important

\* Corresponding authors. Tel.: +852 34117074; fax: +852 34117348 (W.-Y. Wong).

E-mail addresses: [lamlam\\_ho2004@yahoo.com.hk](mailto:lamlam_ho2004@yahoo.com.hk) (C.-L. Ho), [rwywong@hkbu.edu.hk](mailto:rwywong@hkbu.edu.hk) (W.-Y. Wong), [xiezy\\_n@ciac.jl.cn](mailto:xiezy_n@ciac.jl.cn) (Z. Xie).

in order to achieve a better confinement of charge recombination region and, therefore, a better efficiency, can be achieved in a mul-

tilayer device. One simple and useful method for the construction of OLEDs employs a bilayer structure comprising a hole-transport



**Scheme 1.** Synthetic routes to cyclometalating ligands  $L_1$ – $L_{10}$ .

layer and an electron-transport layer, with one or both layers being luminescent [28]. The durability, i.e. thermal and morphological stability of deposited films, is another important factor that has a dramatic influence on the physical performance of OLEDs [29]. It is well recognized that the thermal stability or glassy-state durability of organic compounds can be greatly improved upon incorporation of a carbazole moiety in the core structure [30–32]. Therefore, thermally and morphologically stable dyes with hole-transporting (HT) and light-emitting carbazole chromophore are a preferred choice for the fabrication of OLED devices. Due to the fact that the nature of cyclometalating ligands can influence drastically the lowest energy emitting excited state [33–36], adding the electron-donating or -withdrawing groups and different degree of  $\pi$ -electron conjugation into different positions of the ligands can increase or decrease the amount of electron density at the metal center. The amount of ground state electron density on the metal will subsequently affect the contribution of MLCT character in the lowest energy transition, thus altering the color of emission and radiative lifetime of the excited state of the resulting complexes. Therefore, the purpose of this study is to design a new series of electroactive multi-component Pt(II) cyclometalated complexes with hole-transporting carbazole in which the electroluminescent and HT components are integrated into a single molecule. The electrophosphorescence properties of these metal complexes were also investigated in solution-processed OLEDs.

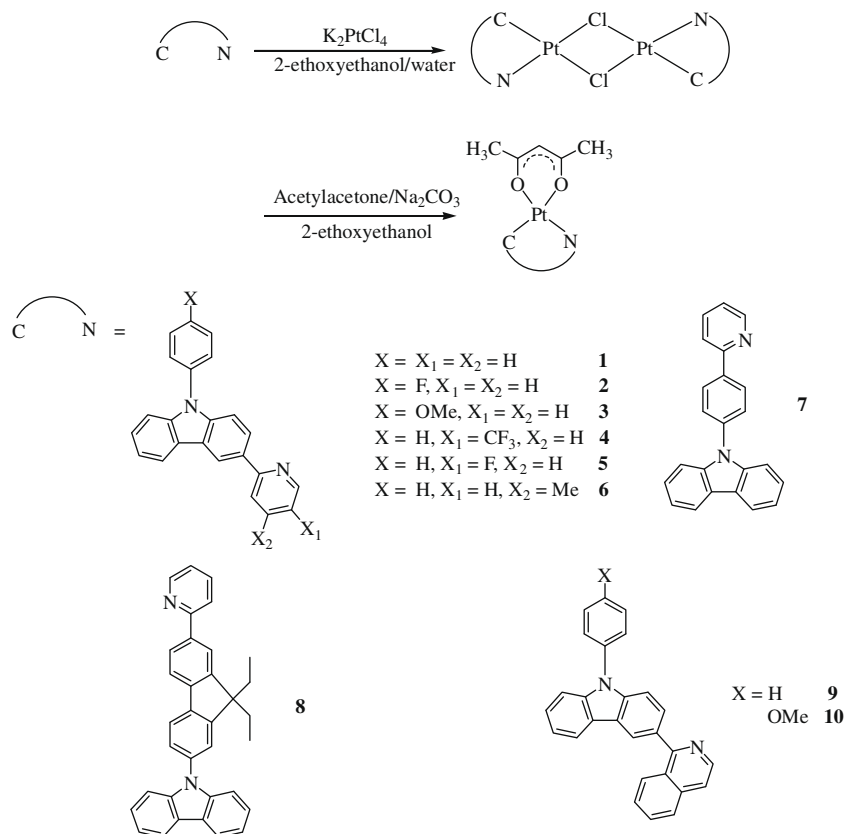
## 2. Results and discussion

### 2.1. Preparation and characterization

A series of carbazole-based cyclometalating ligands **L**<sub>1</sub>–**L**<sub>10</sub> were synthesized according to the reaction steps shown in Scheme 1

[37–42]. **L**<sub>1</sub>–**L**<sub>3</sub> can be obtained from *N*-arylation of carbazole by the modified Ullmann condensation between carbazole and the appropriate *p*-iodoarene using CuI/phen/KOH as the catalyst combination. The desired *N*-arylated 3-bromocarbazole precursors can be readily synthesized from the reaction of the corresponding carbazoles with one stoichiometric amount of *N*-bromosuccinimide (NBS). These compounds were then converted into their cyclometalating partners **L**<sub>1</sub>–**L**<sub>3</sub> by using Pd-catalyzed Stille-coupling reaction with 2-(tributylstannyl)pyridine [43]. The X group spans from H to F and OMe. Pyridyl-substituted 9-phenyl-3-(pyridin-2-yl)carbazoles **L**<sub>4</sub>–**L**<sub>6</sub> were synthesized from palladium-catalyzed Suzuki cross coupling [44–47] of commercially available 2-chloro-5-trifluoromethylpyridine, 2-chloro-5-fluoropyridine or 2-chloro-4-methylpyridine with 9-phenylcarbazole-3-boronic acid, respectively [48,49]. For **L**<sub>7</sub>–**L**<sub>8</sub>, the *N*-arylation of carbazole was carried out by the Ullmann condensation of carbazole with 1-bromo-4-iodobenzene and 2-bromo-7-iodo-9,9-diethylfluorene [50] to give 9-(4-bromophenyl)carbazole and 9-(7-bromo-9,9-diethylfluorenyl)carbazole which can then undergo Stille-coupling protocol with 2-(tri-*n*-butylstannyl)pyridine to afford **L**<sub>7</sub> and **L**<sub>8</sub> which carries a cyclometalating 2-phenylpyridine site for coordination with metal groups. For the isoquinoline-based cyclometalating ligands **L**<sub>9</sub>–**L**<sub>10</sub>, 3-bromo-9-phenylcarbazole and 3-bromo-9-(4-methoxyphenyl)carbazole were first converted to their 3-boronic acid derivatives, which then underwent subsequent Suzuki coupling reactions with 1-chloroisoquinoline to give the desired ligands **L**<sub>9</sub>–**L**<sub>10</sub>.

The chelating cyclometalating ligands **L**<sub>1</sub>–**L**<sub>10</sub> were then used to synthesize a series of new Pt(II) complexes. The targeted Pt(II) emitting materials (Scheme 2) were obtained via two distinctive pathways as previously reported [6]. The first one involves heating the K<sub>2</sub>PtCl<sub>4</sub> salt with 2.5 equivalents of the cyclometalating ligands



Scheme 2. Synthetic routes to new platinum(II) complexes **1**–**10**.

in a 3:1 mixture of 2-ethoxyethanol and water to 80 °C. The dimers were isolated without characterization and used directly in the subsequent reactions. The generated Pt(II)  $\mu$ -dichloro-bridged dimers were then cleaved with acetylacetonone (Hacac) in the presence of a base ( $\text{Na}_2\text{CO}_3$ ) in 2-ethoxyethanol at an elevated temperature. Purification of the mixture by silica chromatography furnished the corresponding mononuclear complexes **1–10** in different solid-state colors as air-stable powders in high purity.

All of the complexes are soluble in chlorinated solvents and can be stored without any special precautions. The identities of the products were accomplished through NMR spectroscopic and mass spectrometric methods from which they were shown to consist of well-defined structures. In all cases,  $^1\text{H}$  NMR resonances arising from the protons of the organic moieties were observed. For instance, the *ortho* proton on the pyridyl ring shows a characteristic doublet at the most downfield position in the proton NMR spectrum in each case. The CH resonance of the acac ligand is located typically at around 5.40 ppm. Two distinct methyl protons of acac fragment were observed as a singlet at around 2 ppm. Some of the carbon NMR spectra were not recorded due to the limited solubility of these complexes in deuterated solvents. For the measured  $^{13}\text{C}$  NMR spectra, two sets of non-equivalent methyl carbons of acac groups were observed due to the asymmetrical chemical environments of two sets of carbons restricted by the square-planar geometry of Pt complexes. The formulae of **1–10** were also successfully established by appearance of the intense molecular ion peaks in their positive FAB mass spectra.

**Table 1**Selected bond lengths (Å) and angles (°) around the metal core in **1–4** and **8–10**.

	Pt–N	Pt–C	Pt–O	C–Pt–N	O–Pt–O
<b>1</b>	1.996(5)	1.953(6)	2.106(4) 1.999(4)	81.8(2)	91.4(2)
<b>2</b>	1.988(5)	1.963(6)	2.108(5) 2.003(4)	81.4(2)	91.5(2)
<b>3</b>	1.999(4)	1.961(4)	2.094(3) 2.004(3)	81.8(2)	91.4(1)
<b>4<sup>a</sup></b>	1.986(4) [1.997(4)]	1.963(5) [1.966(5)]	2.099(3), 1.993(3) [2.099(3), 1.990(3)]	81.5(2) [81.4(2)]	91.9(1) [91.5(1)]
<b>8</b>	1.986(4)	1.972(4)	2.086(3) 1.995(3)	81.2(2)	91.8(1)
<b>9</b>	1.986(3)	1.953(4)	2.094(3) 2.006(3)	80.3(2)	91.3(1)
<b>10</b>	2.000(9) [1.976(8)]	1.96(1) [1.96(1)]	2.104(8), 2.019(7) [2.105(8), 2.012(7)]	80.3(2) [80.8(4)]	91.4(3) [90.4(3)]

<sup>a</sup> The values for the second independent molecule per asymmetric unit are shown in parentheses.

## 2.2. Crystal structures

To further establish their molecular structures, a majority of these Pt(II) complexes (**1–4** and **8–10**) were subjected to X-ray single-crystal diffraction studies. Most of them can rapidly form microcrystalline solids from solvent mixtures of chlorinated hydrocarbons and hexane. Perspective drawings of complexes **1–4** and **8–10** are shown in Fig. 1 and key bonding parameters

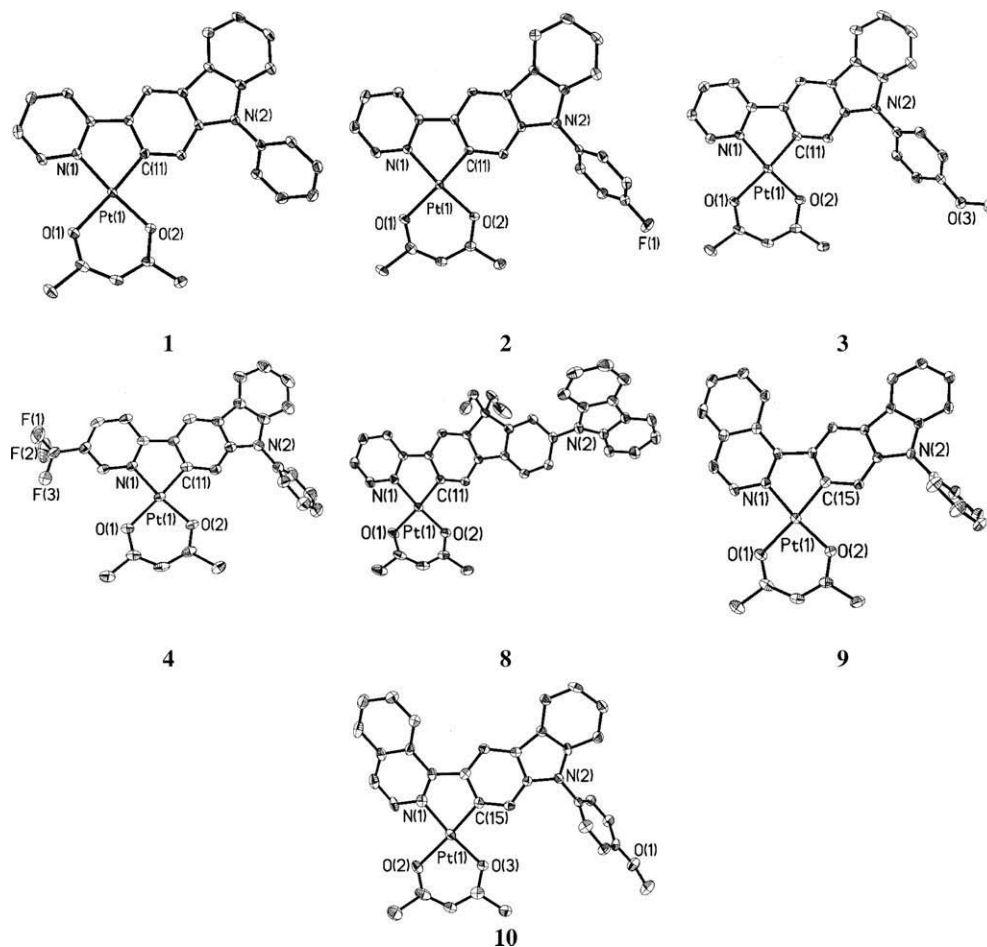


**Fig. 1.** ORTEP drawings of **1–4** and **8–10**, with thermal ellipsoids shown at the 25% probability levels. Labels on carbon atoms (except for those bonded to Pt) and all hydrogen atoms are omitted for clarity.

are given in Table 1. Due to the bulkiness of carbazolyl chromophores, all of the structures do not show the  $\pi$ - $\pi$  stacking interactions between molecules. In all cases, the platinum center exhibits the expected distorted square-planar coordination and the phenyl-pyridyl metallacycle is essentially coplanar. There is a very little distortion away from the square plane, and the C-Pt-N and O-Pt-O chelate planes are only slightly bowed. The bond length of Pt-N [1.975(3)–2.000(9) Å] is slightly longer compared to that of common Pt-N bonds because this N is opposite to the acac O atom having a weak *trans* influence. The two Pt-O bond lengths are different, the longer of the two consistently corresponding to that disposed *trans* to the cyclometalating carbon. This is a reflection of the stronger *trans* influence with carbon

[2.086(2)–2.108(5) Å] than with nitrogen atom [1.990(3)–2.019(7) Å], a feature commonly observed for other chelating diketonato complexes containing bidentate cyclometalating ligands [1,51–56] and the bite N-Pt-C angles are similar to those found for related (C^N)Pt-type complexes [6]. For **4** and **10**, two unique independent molecules were observed in the asymmetric unit of the unit cells in each case.

### 2.3. Photophysical and thermal properties

Since good thermal stabilities of the compounds are very important for the OLED applications, the onset decomposition temperatures ( $T_{\text{decomp}}$ ) of the new compounds were determined from

**Table 2**  
Photophysical and thermal data for **1–4**.

	Absorption (293 K)		Emission (293 K)			Emission (77 K)		$T_{\text{dec}}$ (°C)
	$\lambda_{\text{abs}}$ (nm) <sup>a</sup>	$\epsilon$ (M <sup>-1</sup> cm <sup>-1</sup> ) <sup>a</sup>	$\lambda_{\text{em}}$ (nm)	$\Phi_{\text{p}}$ <sup>b</sup>	$\tau_{\text{p}}$ [ $\mu\text{s}$ ] <sup>c</sup>	$\lambda_{\text{em}}$ (nm)	$\tau_{\text{p}}$ ( $\mu\text{s}$ ) <sup>c</sup>	
<b>1</b>	259	(1.99)	493	0.11	0.13	486	27.9	324
	300	(2.66)	525sh			493sh		
	327	(2.63)				513sh		
	366	(0.72)				524		
	373	(0.67)				557sh		
	408	(0.04)						
<b>2</b>	259	(2.02)	493	0.12	0.12	491	21.7	312
	299	(2.65)	524sh			501sh		
	327	(2.63)				529		
	366	(0.70)				561sh		
	374	(0.58)						
	408	(0.18)						
<b>3</b>	261	(4.19)	495	0.08	0.14	494	25.2	289
	300	(4.81)	525sh			503sh		
	327	(4.69)				524sh		
	373	(1.48)				532		
	409	(0.75)				563sh		
<b>4</b>	264	(4.64)	520	0.16	0.13	499	9.7	312
	304	(7.32)	551sh			519sh		
	336	(4.07)				537sh		
	393	(2.53)				613sh		
	432	(0.17)						
<b>5</b>	263	(9.65)	504	0.1	0.09	493	23.5	234
	301	(13.60)	533sh			502sh		
	333	(8.71)				533		
	377	(2.64)				572sh		
	422	(0.79)						
<b>6</b>	256	(4.71)	488	0.1	0.14	484	18.7	350
	303	(5.52)	519sh			501sh		
	323	(6.11)	565sh			511sh		
	363	(1.97)				522		
	406	(0.93)				560sh		
<b>7</b>	261	(11.65)	502	0.23	0.35	497	14.7	318
	293	(5.70)	536sh			540		
	329	(4.07)				575sh		
	345	(4.31)						
	401	(1.45)						
<b>8</b>	259	(11.86)	547	0.1	0.12	511	16.5	320
	294	(9.76)	589sh			558		
	344	(10.19)				608sh		
	405	(3.47)						
	422	(3.18)						
<b>9</b>	262	(3.87)	606	0.06	d	564	22.7	297
	321	(3.34)	650sh			613		
	334	(2.71)				675sh		
	384	(1.25)						
	413	(1.34)						
	469	(0.61)						
<b>10</b>	258	(3.07)	607	0.05	d	595	14.5	294
	322	(2.62)	650sh			647		
	385	(0.49)				706sh		
	414	(1.02)						
	467	(0.87)						

<sup>a</sup>  $\epsilon$  values ( $10^4 \text{ M}^{-1} \text{ cm}^{-1}$ ) are shown in parentheses.

<sup>b</sup> Measured in  $\text{CH}_2\text{Cl}_2$  relative to *fac*-[Ir(ppy)<sub>3</sub>] ( $\Phi_{\text{p}} = 0.40$ ),  $\lambda_{\text{ex}} = 400 \text{ nm}$ .

<sup>c</sup> In  $\text{CH}_2\text{Cl}_2$  at 293 K. sh = shoulder.

<sup>d</sup> Not determined due to the inherent instrumental limitation. sh = shoulder or broad peak.

thermogravimetric analysis (TGA) under a nitrogen stream. From the onset of the TGA curves, all the complexes show very good thermal stabilities with their  $T_{\text{decomp}}$  ranging from 234 to 350 °C. The first weight loss of the compounds was mostly due to dissociation of the ancillary acac ligand.

The absorption spectra of all the metallized complexes were measured in  $\text{CH}_2\text{Cl}_2$  at room temperature and the pertinent data are presented in Table 2. In common with most cyclometalated Pt(II) complexes the absorption spectra can be divided into two regions: the strong absorptions in the UV region (<350 nm) are derived from a typical ligand-centered  $\pi-\pi^*$  transition because the corresponding transitions were also observed in the free ligands. For example, the lowest energy  $\pi-\pi^*$  absorption of complex **1** was found at 327 nm while the corresponding free ligand **L**<sub>1</sub> appeared at 322 nm. Although these transitions are slightly red-shifted from their corresponding free ligands, they are not solvatochromic. These are only attributed to the perturbation from the metal. Metal-centered, d-d transitions are not observed for these complexes. It is believed that the strong ligand field of the C<sup>^</sup>N ligands shifts the d-d transitions to high energy, putting them under the more intense ligand-centered and metal-to-ligand charge transfer (MLCT) transitions [57,58]. Therefore, the second regions that extend to the visible region are conventionally assigned as mixing among singlet and triplet metal-to-ligand charge transfer transitions (<sup>1</sup>MLCT and <sup>3</sup>MLCT) and to a certain extent with intraligand <sup>3</sup> $\pi-\pi$  transitions through the spin-orbit coupling by the hea-

vy metal center, which are not observed in the free ligands. The substituents on the 9-phenyl ring of 2-[3-(N-arylcarbazolyl)]pyridine have no significant influence on the absorption properties of the complexes **1–3** as well as their isoquinoline counterparts **9–10**. The lower-lying band is shifted upon the attachment of different substituents on the pyridyl ring in the order: **4** ( $X_2 = \text{CF}_3$ ,  $\lambda_{\text{max}} = 432 \text{ nm}$ ) > **5** ( $X_2 = \text{F}$ ,  $\lambda_{\text{max}} = 422 \text{ nm}$ ) > **1** ( $X_1 = X_2 = \text{H}$ ,  $\lambda_{\text{max}} = 408 \text{ nm}$ ) > **6** ( $X_1 = \text{Me}$ ,  $\lambda_{\text{max}} = 406 \text{ nm}$ ). These results agree with the literature data [59] that introduction of electron-donating groups to the pyridine ring can cause a decrease of the HOMO level and a larger band gap than the unsubstituted one and vice versa. Fig. 2 shows the absorption spectra of **1–10**.

While all of the ligands fluoresce in the blue, their Pt complexes emit strong photoluminescence (PL) originated from a triplet manifold at room temperature in fluid solution accompanied by large Stokes shifts (>100 nm). No fluorescence could be detected for each of the complexes. The room temperature phosphorescence spectra of **1–10** are depicted in Fig. 3. The colors of the complexes span from green to yellow, orange and red. Fig. 4 shows the color-tuning strategy achieved by the carbazolyl ligands in our Pt complexes. The emission spectra possess distinctive vibronic like progression which we can expect a significant amount of <sup>3</sup>MLCT state mixing with the ligand-centered <sup>3</sup> $\pi-\pi$  transitions [60,61]. As for the absorption features, the change of substituents on the 9-phenyl ring of carbazole has no profound effect on the emission maximum. The emission energies are, however, strongly sensitive to

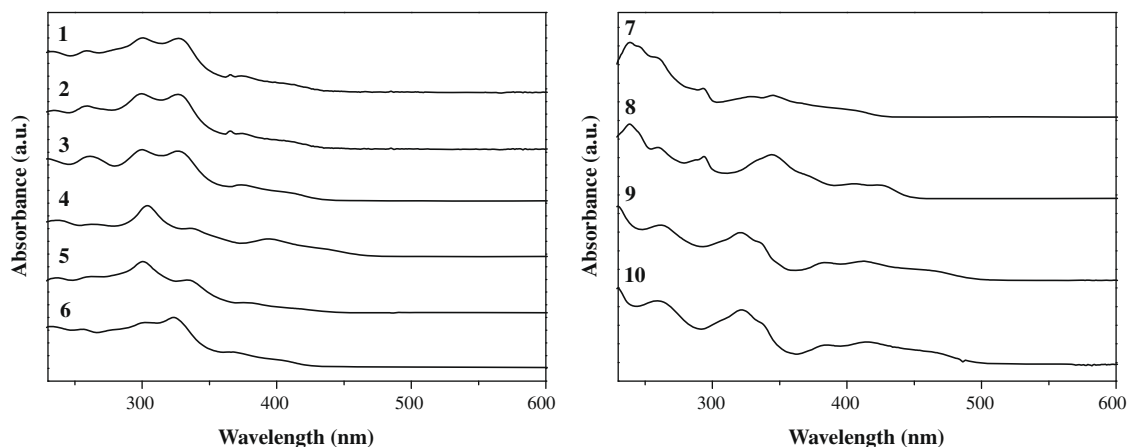


Fig. 2. Absorption spectra of **1–10** in  $\text{CH}_2\text{Cl}_2$  at 293 K.

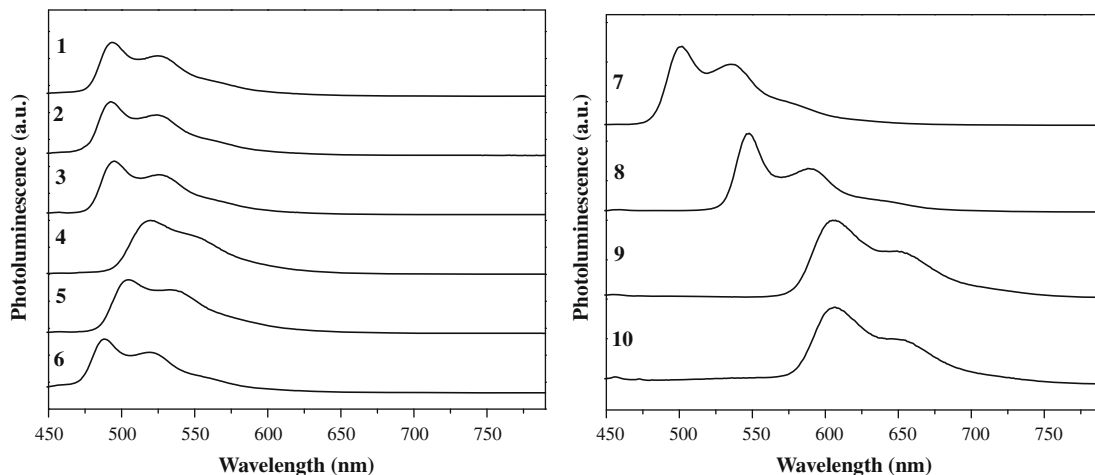


Fig. 3. Photoluminescence (PL) spectra of **1–10** in  $\text{CH}_2\text{Cl}_2$  at 293 K.

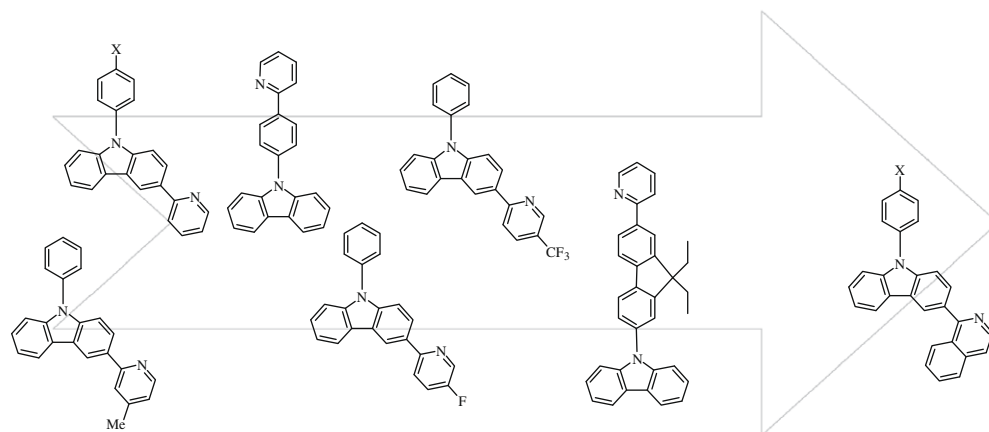


Fig. 4. Color-tuning strategy in cyclometalated Pt(II) complexes.

the electronic properties of substituents on the pyridine ring. A weakly  $\sigma$ -donating methyl group in the 4-position on the pyridyl ring (with respect to the Ir–N bond) results in a slight blue shift of 9 nm for **6**. The electron-withdrawing F group in the 5-position causes a bathochromic shift on the emission (complex **5**), and the stronger  $\text{CF}_3$   $\sigma$ -electron acceptor imparts a more substantial red shift for **4**. Therefore,  $\lambda_{\text{em}}$  decreases in the order: **4** > **5** > **1** > **6**. Since the LUMO level is principally located on the electron deficient pyridyl ring [59,62], substitution of an electron-withdrawing group would decrease the HOMO–LUMO energy gap, thus a red shift of the emission was observed. This sensitivity of transition energy to the substitution effect on the pyridyl ring has been previously observed in related tris(cyclometalated) iridium complexes [59,63–69]. For the two pairs of geometrical isomers (**1** versus **7** and **2** versus **5**), we note an obvious ligand or substituent effect on the emission position. There is a red shift of  $\sim 10$  nm in  $\lambda_{\text{em}}$  upon going from **1** (493 nm) to **7** (502 nm) or **2** (493 nm) to **5** (504 nm). On the other hand, incorporating a more conjugative cyclometalating ligand on the phenyl ring also enables the tuning of the energy of the emissive state for this kind of Pt complexes. When fluorene was inserted between the pyridine ring and the carbazole unit (complex **8**), a pronounced red shift in  $\lambda_{\text{em}}$  was observed, i.e. **8** (547 nm) > **7** (502 nm). An increase in the conjugation of the phenyl ring would decrease the LUMO level, leading to a red shift in wavelength. For the isoquinoline derivatives, large red shifts can be found by extending the size of the  $\pi$ -conjugated fused ring sys-

tem in the heterocycle and they all emit red phosphorescence with a maximum at 606 and 607 nm for **9** and **10**, respectively.

All of the Pt complexes are intensely emissive at 77 K in a rigid matrix. Most of the complexes show some extent of rigidochromic blue shifts compared to their room temperature emission features. Complexes **1–7** show well-defined spectra with many separated vibronic attenuations. For example, the spectrum of complex **1** consists of two main sets of bands with well-defined structure, one with  $\lambda_{\text{em}} = 486$  nm and the other one with  $\lambda_{\text{em}} = 524$  nm. However, different behavior was observed in **8–10** which displayed less vibronic attenuations. Fig. 5 illustrates the representative emission spectra of **1**, **4**, **8** and **9** at 77 K. Substituents effects on pyridyl ring are less pronounced for altering the phosphorescence emission energies at low temperature.

We further probed the photophysical properties of **1–10** by measuring their PL quantum yields ( $\Phi_{\text{p}}$ ) in dilute degassed  $\text{CH}_2\text{Cl}_2$  solutions. Among all the green/yellow compounds **1–7**, complex **7** has the highest room temperature quantum efficiency of 23%, which is higher than that for its isomeric compound **1** (11%). An increase in  $\Phi_{\text{p}}$  (16%) was observed when a trifluoromethyl group was attached to the pyridine ring. As the energy of emission decreases, a corresponding general decrease in  $\Phi_{\text{p}}$  at room temperature is observed, except for the fluorene-containing complex **8** which has  $\Phi_{\text{p}}$  of 10%. This may be attributed to the fact that fluorene is a well-known functional core possessing high quantum efficiency among all the organic species. The lifetimes of the complexes at room temperature and 77 K were also measured at infinite dilution under nitrogen atmosphere. They generally feature long-lived excited states in the sub-microsecond region at room temperature, signaling that the emissions originate from a mixed  $^3\text{LC}/^3\text{MLCT}$  state. The phosphorescence lifetimes at 77 K are much longer than those at room temperature since the non-radiative decay rates usually decrease with lowering temperature [36].

#### 2.4. Density functional theory (DFT) calculations

To study the electronic structures and understand the nature of excited states of our new Pt(II) phosphors, density functional theory (DFT) and time-dependent DFT (TDDFT) calculations were carried out using B3LYP hybrid functional theory for selected molecules. Our TDDFT calculations show that the  $S_0 \rightarrow S_1$  transitions correspond to the HOMO  $\rightarrow$  LUMO transitions with non-zero oscillator strengths (Table 3). Therefore, we will place our special emphasis on the HOMO–LUMO analyses in the following discussion. The calculations show that HOMOs consist of the metal d orbital mixing with the  $\pi$  orbitals of the phenyl ring that is directly bonded to the metal center. The LUMOs correspond to the lowest

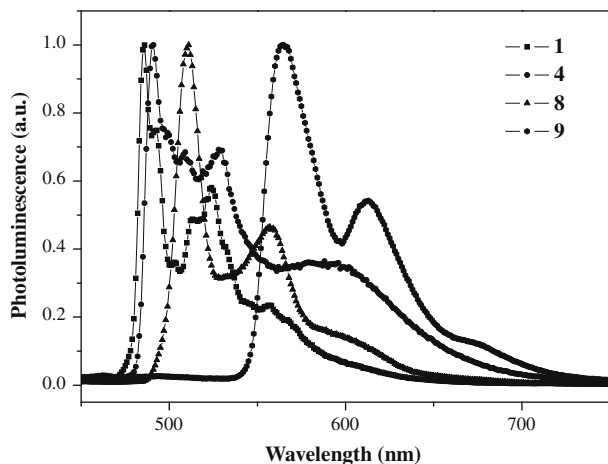


Fig. 5. PL spectra of **1**, **4**, **8** and **9** in  $\text{CH}_2\text{Cl}_2$  at 77 K.

**Table 3**Percentage contribution of the metal  $d_{\pi}$  orbitals to HOMO and LUMO together with the TDDFT calculation results.

Compound	Contribution of d orbitals to HOMO (%)	Contribution of d orbitals to LUMO (%)	The largest coefficient in the CI expansion of the $S_1$ state <sup>a</sup>	The oscillator strength ( $f$ ) of the $S_0 \rightarrow S_1$ transition
<b>1</b>	21.4	2.9	H → L: 0.65	0.012
<b>2</b>	20.6	3.4	H → L: 0.63	0.010
<b>3</b>	16.0	3.1	H → L: 0.53	0.014
<b>4</b>	19.1	3.2	H → L: 0.61	0.016
<b>8</b>	3.9	5.6	H → L: 0.53	0.172
<b>9</b>	23.5	2.8	H → L: 0.68	0.031
<b>10</b>	15.4	3.3	H → L: 0.60	0.015
<b>[Pt(FI-py)acac]</b>	23.8	5.8	H → L: 0.65	0.056

<sup>a</sup> H → L represents the HOMO to LUMO transition. CI stands for configuration interaction.

$\pi^*$  orbital from the Pt-bonded pyridine ring. The HOMO and LUMO levels have  $\pi$  symmetry, with opposite phases above and below the molecular plane. That is, the HOMO consists of a mixture of phenyl, Pt, and acac orbitals while the LUMO is predominantly 2-phenylpyridyl in character. From Fig. 6, it is clear that the HOMO–LUMO gaps calculated for **1–3** are close to each other, revealing that the HOMO and LUMO levels are not influenced by the F and OMe substituents on the aryl ring of carbazole. In contrast, adding an electron-withdrawing  $\text{CF}_3$  group on the pyridine ring affects the LUMO level significantly, resulting in a marked decrease in energy gap. Much smaller calculated band gap values were observed in **9** and **10**, consistent with the optical studies. The HOMO stability and emission energy are almost invariant of the identity of X on the aryl ring of carbazole. For **8**, the HOMO showing a greater delocalization over the aryl ligand leads to a less extent of metal d orbital mixing. The greater delocalization due to the participation of orbitals from the carbazolyl substituent gives a smaller HOMO–LUMO gap in **8** when compared with that in **[Pt(FI-py)acac]** (Fig. 7) [70].

### 2.5. Electrochemical and electronic characterization

The electrochemical properties of **1–10** were examined using cyclic voltammetry, and the redox data are given in Table 4. All of the electrochemical potentials reported here were measured relative to an internal ferrocene standard ( $\text{Cp}_2\text{Fe}/\text{Cp}_2\text{Fe}^+$ ) [71]. All of the Pt complexes show reversible reduction and irreversible oxidation waves. This electrochemical behavior is similar to that reported for related (C^N)Pt-type complexes [6]. As pointed out

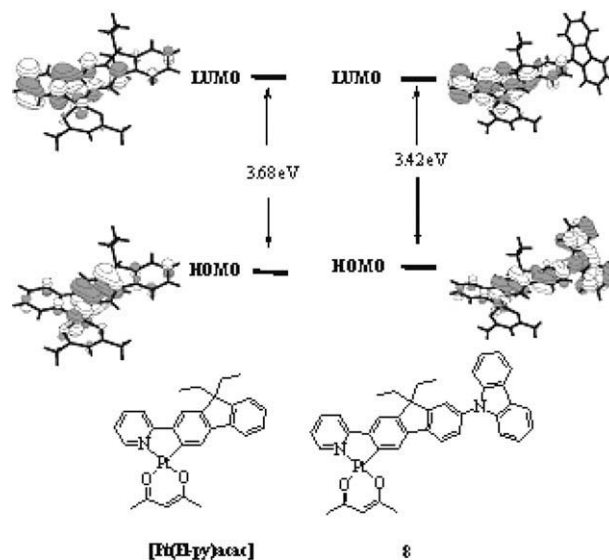


**Fig. 7.** Contour plots of dominant excitation orbitals of fluorene-containing platinum(II) complex **8** and its non-carbazole parent species **[Pt(FI-py)acac]**.

above, the HOMO of cyclometalated Pt(II) complexes typically consists of a mixture of phenyl, Pt, and acac orbitals while the LUMO is predominantly pyridyl in character [6]. Unfortunately, electrochemical oxidation of Pt(II) complexes is typically an irreversible

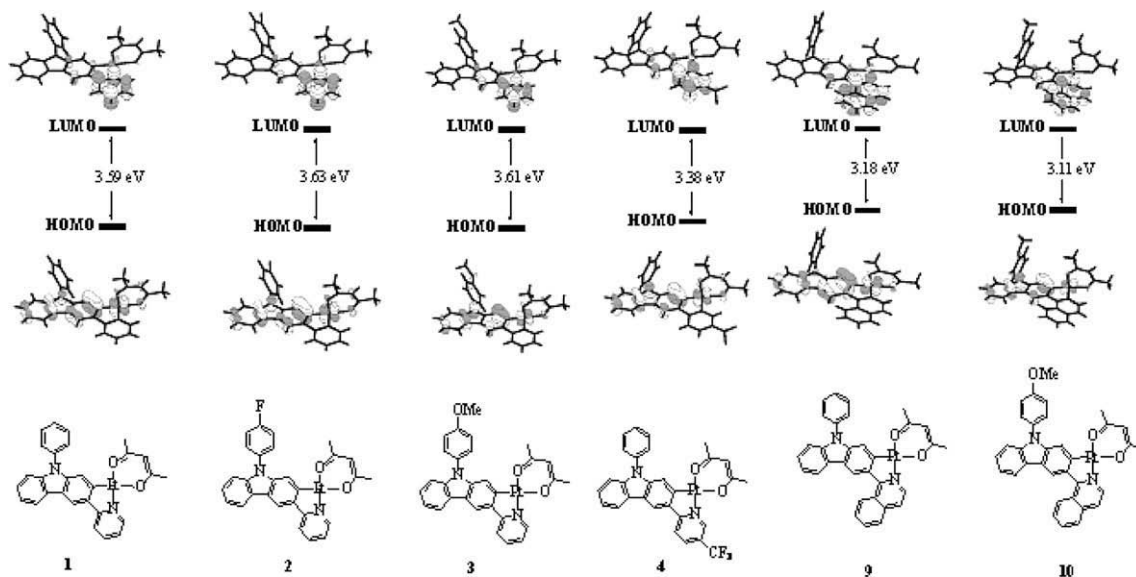


**Fig. 6.** Contour plots of dominant excitation orbitals of some of the platinum(II) complexes.

**Table 4**  
Electrochemical properties and frontier orbital energy levels of **1–10**.

Complex	$E_{1/2}^{\text{ox}}$ (V) <sup>a</sup>	HOMO (eV) <sup>b</sup>	$E_{1/2}^{\text{red}}$ (V) <sup>a</sup>	LUMO (eV) <sup>c</sup>
<b>1</b>	0.28	−5.08	−2.52	−2.28
<b>2</b>	0.30	−5.10	−2.52	−2.28
<b>3</b>	0.29	−5.09	−2.54	−2.26
<b>4</b>	0.24, 0.44	−5.03	−2.21, −2.61	−2.59
<b>5</b>	0.34	−5.14	−2.40	−2.40
<b>6</b>	0.29	−5.09	−2.62	−2.18
<b>7</b>	0.32	−5.11	−2.40	−2.40
<b>8</b>	0.38	−5.18	−2.36, −2.79	−2.44
<b>9</b>	0.28	−5.08	−2.12, −2.76	−2.68
<b>10</b>	0.28	−5.08	−2.13, −2.76	−2.67

<sup>a</sup> 0.1 M [Bu<sub>4</sub>N]PF<sub>6</sub> in THF, scan rate 100 mV s<sup>−1</sup>, versus Fc/Fc<sup>+</sup> couple.

<sup>b</sup> Irreversible wave.

<sup>c</sup> Reversible wave.

process caused by solvent coordination to the open coordination site on the metal center (i.e. susceptible to nucleophilic attack by solvents) and subsequent ligand rearrangement [33,35,36]. Therefore, the  $E_{\text{ox}}$  values do not necessarily represent the true thermodynamic potential for removing an electron from the complexes. In order to get a more meaningful interpretation, we look at the details of reduction processes of the complexes. All of the complexes show a reduction peak in the range of −2.02 to −2.62 V. Complex **1** has the  $E_{\text{red}}$  value (−2.52 V) more negative than [Pt(ppy)(acac)] (−2.39 V) [6], suggesting that the LUMO level (ca. −2.28 and −2.41 eV for **1** and [Pt(ppy)(acac)], respectively) is destabilized by the inclusion of carbazole unit. This is mainly attributed to the poorer electron-accepting property of carbazole as compared to the phenyl ring. From these results, we observe that the reduction potentials of these complexes are strongly sensitive to the nature of substituents on the pyridyl ring. When electron-donating groups (such as 4-methyl-substituted group in **6**) were attached to the pyridyl ring, destabilized LUMO level was observed relative to the unsubstituted one in **1**. On the other hand, addition of electron-withdrawing substituents, such as fluorine atom (in **5**) and trifluoromethyl group (in **4**) stabilized the LUMO levels. Therefore, the LUMO level decreases in the order of **6** (−2.18 eV) > **1** (−2.28 eV) > **5** (−2.40 eV) > **4** (−2.58 eV). This is in agreement with some of the literature data [59,62] and a red shift in the emission wavelength often occurs owing to a lowering of the LUMO energy level.

However, substituents on the 9-phenyl ring of carbazole have no marked influence on the redox properties of the complexes. Similar  $E_{\text{red}}$  was recorded for **1–3**. Complex **7** has a reduction wave at −2.40 V, making it 110 mV easier to reduce than that for **1**. There is a gentle decrease in the reduction potential along the sequence **7** (−2.40 V) > **8** (−2.36 V) which is mainly caused by the increase of  $\pi$ -conjugation in the cyclometalating ligands that leads to a greater stabilization of the negative charge on the more delocalized  $\pi$ -orbital system. This means that increasing the  $\pi$  electron extension in the C<sup>^</sup>N ligands renders the complexes easier to reduce. Replacement of the pyridyl ring by isoquinoline also shows stabilized LUMO levels: **9** (−2.68 eV)  $\approx$  **10** (−2.67 eV).

As compared to [Pt(ppy)acac] (HOMO: −5.34 eV) [6,36], the HOMO levels of **1–10** are all elevated when the electron-rich and -donating carbazolyl units are attached to the pyridyl rings, signaling that they have a lower ionization potential than their ppy congener, leading to a better hole injection (HI) and/or HT ability and thus our complexes can serve as dual functional triplet emitters. Energetics governing the HOMO and LUMO levels of the materials are usually crucial for efficient OLED architecture. The HOMO energy levels of our carbazole-containing compounds lie within those of ITO (HOMO: −4.70 eV) [72], PEDOT:PSS (−5.0 eV) [73] and Alq<sub>3</sub> (−6.00 eV) [74], while the LUMO energy levels lie above Alq<sub>3</sub>

(−3.0 eV). The close match of the HOMO levels of our Pt dyes and the Fermi level of PEDOT likely results in a good HI contact and an improvement in the hole carrier balance in the OLEDs even without the need for an additional HT layer (vide infra).

## 2.6. Electrophosphorescent OLED characterization

Today, OLED is believed to be one of the most promising technologies for flexible passive- and active-matrix flat panel displays because OLEDs can be easily fabricated over large-area plastic substrates at room temperature and low cost. Therefore, materials that can be spun into uniform and thin films are industrially demanding. While we expect our Pt compounds here are sublimable for the fabrication of doped electrophosphorescent multilayered OLEDs, our ultimate goal, however, is to make some solution-processed devices for the realization of large-area displays. The emitting layers for all of the devices were prepared by using the relatively cheaper solution-processed spin-coating technique. It should be noted that CBP itself normally cannot be spin-coated from solution to form good-quality thin films. When the dopant concentration is very low (e.g. <3 wt-%), the CBP host is prone to crystallization in the as-prepared films and the devices short easily. This illustrates that the good film-forming properties of our bulky metal phosphors can ensure a good chemical compatibility with the CBP host, resulting in a homogeneous distribution of each Pt dopant in CBP [75]. In this way, various OLEDs were fabricated by spin-coating the selected Pt(II) materials onto indium tin oxide (ITO) coated glass, which is used as an anode. The configuration of Pt-based devices and the molecular structures of the compounds used in these devices are depicted in Fig. 8. A layer of poly(3,4-ethylenedioxythiophene):poly(styrenesulfonate) (PEDOT:PSS) was adopted which can also be used as the HI layer to smooth the ITO surface [76] and reduce interfacial surface area and lower the leakage current. A layer of conductive host material 4,4'-N,N'-dicarbazolebiphenyl (CBP) doped with different concentrations (3–12 wt-%) of Pt dyes was employed to optimize the device efficiency. We have used CBP as the host because of its proven performance as host for Pt complexes and theoretical confirmation of favorable triplet energy [77–79]. But the conventional HT layer of NPB was not necessary in fabricating our devices. This can, to a certain extent, corroborate with the improved HI/HT properties of our materials from the PEDOT:PSS layer. Then the emitting layer composed of the triplet dopant and CBP host was deposited. The devices consist of a thin layer of 2,9-dimethyl-4,7-diphenyl-1,10-phenanthroline (BCP) for hole and exciton blocking to confine the recombination zone inside the doped CBP layer; a layer of electron-transporting tris[8-hydroxyquinoline] (Alq<sub>3</sub>) for electron-transport [80], and LiF as an electron injection layer. This configuration was adopted from those reported previously [81]. Important device performance characteristics are collected in Table 5.

OLEDs using phosphors **2** and **3** exhibited bright green emission when a positive bias was applied between the electrodes. Fig. 9 shows the voltage-independent electroluminescence (EL) spectra at different doping concentrations. The EL spectra are nearly coincident with the PL spectra of the corresponding complexes in the polymer matrix at room temperature when the doping concentration is low (e.g. at 3 wt-%), indicating an effective energy transfer from the host exciton to the phosphor upon electrical excitation and the effective hole-blocking effect of BCP. The blue emission from the host and HT layers is negligible. However, emission from aggregate states is observed from both devices and the extent of aggregation is increased with increasing doping concentrations so that broad emission bands appear at the lower energy shoulder. For device **B4** with dopant **3** at 12 wt-%, the EL shows three peaks, the first two being vibronic transitions from the parent dopant (496 and 536 nm), while a new aggregate emission band appears

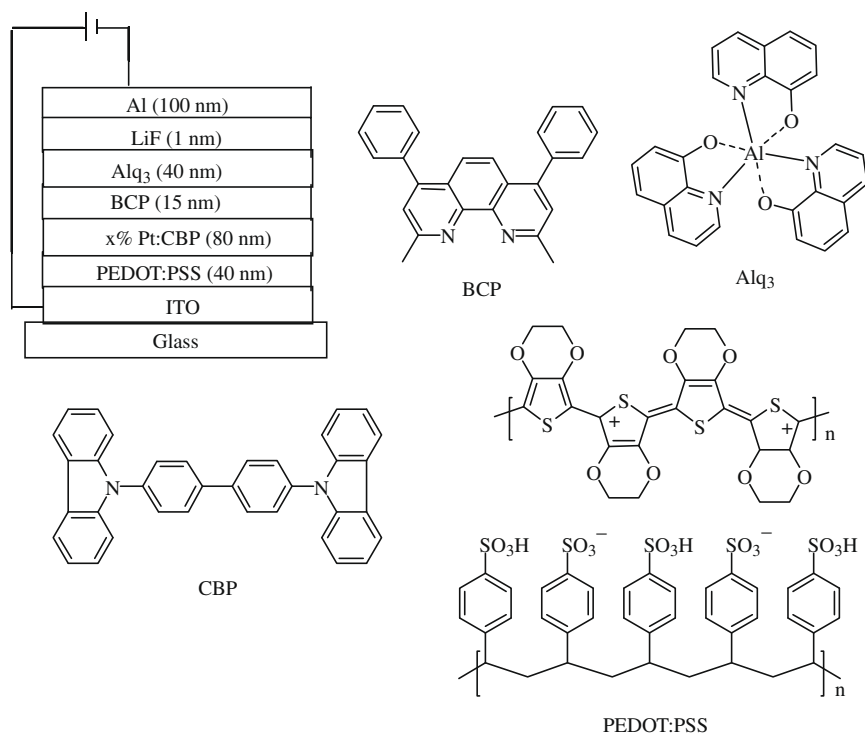


Fig. 8. The general structure for Pt-doped OLED devices and the molecular structures of the relevant compounds used.

Table 5  
Performance of Pt-doped electrophosphorescent OLEDs.

Device	Phosphor (wt.-%)	$V_{\text{turn-on}}$ (V)	Luminance ( $\text{cd}/\text{m}^2$ )	$\eta_{\text{ext}}$ (%) <sup>a</sup>	$\eta_{\text{L}}$ ( $\text{cd}/\text{A}$ ) <sup>a</sup>	$\eta_{\text{p}}$ ( $\text{lm}/\text{W}$ ) <sup>a</sup>	$\lambda_{\text{em}}$ (nm) (x, y) <sup>c</sup>
A1	2 (3)	7.0	1173 (12.5)	0.22 (11.0)	0.64 (11.0)	0.18 (11.0)	496sh, 527 (0.34, 0.55)
A2	2 (6)	8.6	1363 (14)	0.39 (11.0)	1.10 (11.0)	0.33 (10.0)	494, 523sh (0.35, 0.54)
A3	2 (9)	9.7	1147 (16)	0.28 (14.0)	0.77 (14.0)	0.18 (13.0)	496sh, 527 (0.38, 0.54)
A4	2 (12)	9.8	1286 (16.5)	0.36 (14.0)	0.99 (14.0)	0.23 (13.0)	496sh, 527 (0.38, 0.54)
B1	3 (3)	7.5	1403 (13.5)	0.43 (12.0)	1.26 (12.0)	0.59 (10.5)	495sh, 526 (0.36, 0.56)
B2	3 (6)	8.3	2059 (15)	0.50 (12.5)	1.40 (12.5)	0.39 (11.0)	495sh, 526, 563sh (0.39, 0.54)
B3	3 (9)	7.7	2271 (14.5)	1.23 (14)	2.80 (12.5)	0.77 (14.0)	495sh, 531, 564sh (0.41, 0.53)
B4	3 (12)	9.3	2376 (16)	0.90 (13.0)	2.39 (16.0)	0.44 (13.0)	499sh, 535sh, 572 (0.43, 0.52)
B5 <sup>b</sup>	3 (3)	5.7	724 (10)	0.17 (8.0)	0.44 (8.0)	0.18 (7.0)	491, 520sh (0.25, 0.45)
B6 <sup>b</sup>	3 (6)	5.7	2135 (10.5)	0.44 (8.0)	1.25 (8.0)	0.49 (8.0)	496, 523sh (0.28, 0.51)
B7 <sup>b</sup>	3 (9)	5.7	1527 (10)	0.50 (8.5)	1.45 (8.5)	0.55 (7.0)	496, 524sh (0.30, 0.53)
B8 <sup>b</sup>	3 (12)	4.1	3223 (10.5)	0.68 (6.5)	2.28 (9.0)	0.96 (6.5)	496, 528sh (0.31, 0.54)
C1	4 (3)	6.5	16550 (16)	1.75 (15.5)	5.99 (15.5)	1.30 (13.0)	515, 543sh (0.32, 0.62)
C2	4 (6)	8.6	11440 (18)	1.53 (17.5)	4.98 (17.5)	0.89 (17.5)	515, 543sh (0.34, 0.61)
C3	4 (9)	7.8	8982 (19)	1.46 (18.0)	4.21 (18.0)	0.81 (16.0)	515, 544sh (0.36, 0.59)
C4	4 (12)	7.9	7627 (20)	1.32 (19.0)	3.73 (19.0)	0.68 (16.5)	515, 548sh (0.38, 0.57)
C5 <sup>b</sup>	4 (3)	4.6	14010 (11.5)	2.36 (7.5)	7.50 (7.5)	3.29 (7.0)	512, 540sh (0.34, 0.59)
C6 <sup>b</sup>	4 (6)	4.2	15970 (12.5)	2.65 (7.0)	8.33 (7.0)	3.89 (6.5)	512, 540sh (0.34, 0.59)
C7 <sup>b</sup>	4 (9)	3.3	16960 (13)	2.77 (8.5)	8.49 (8.5)	3.48 (7.5)	512, 543sh (0.36, 0.59)
C8 <sup>b</sup>	4 (12)	4.3	11910 (13)	2.10 (9.5)	6.41 (9.5)	2.51 (6.5)	512, 543sh (0.36, 0.58)
D1	8 (3)	12.6	1592 (19.5)	0.40 (19.0)	1.13 (19.0)	0.19 (17.5)	547, 586sh, 647sh (0.48, 0.51)
D2	8 (6)	11.9	1601 (22)	0.35 (20.5)	0.92 (20.5)	0.15 (17.0)	547, 590sh, 643sh (0.49, 0.51)
D3	8 (9)	12.4	1359 (22.5)	0.32 (20.0)	0.73 (20.0)	0.12 (19.5)	547, 592sh, 647sh (0.51, 0.49)
D4	8 (12)	12.5	1246 (22)	0.34 (20.0)	0.74 (20.0)	0.14 (14.0)	547, 591sh, 647sh (0.51, 0.49)

<sup>a</sup> Maximum values of the devices. Values in parentheses are the voltages at which the maximum values were obtained.

<sup>b</sup> Spin-coated emissive layer was obtained by using toluene during OLED fabrication.

<sup>c</sup> CIE coordinates shown in parentheses.

near 570 nm. This emission band diminishes as the doping concentration is low. The emission properties of luminescent Pt compounds typically undergo large changes upon going from a dilute solution to the neat solid-state. Intermolecular interactions often lead to emission from a neat solid that is red-shifted in comparison to what is observed from the isolated molecule. This phenomenon is particularly pronounced for Pt(II) complexes coordinated to ligands with conjugated  $\pi$ -systems as the square-planar geometry

of the molecule easily accommodates  $\pi$ -stacking interactions in the solid-state [82–85]. Indeed, generating white light from phosphor–excimer or aggregate emission has been proven effective and leads to simpler device structures than those requiring separate red, green and blue emitters. It is true that a solvent used for film formation could affect the solid molecular packing of the active material. The low-energy emission is becoming more apparent in chloroform-processed devices with increase of dopant concentra-

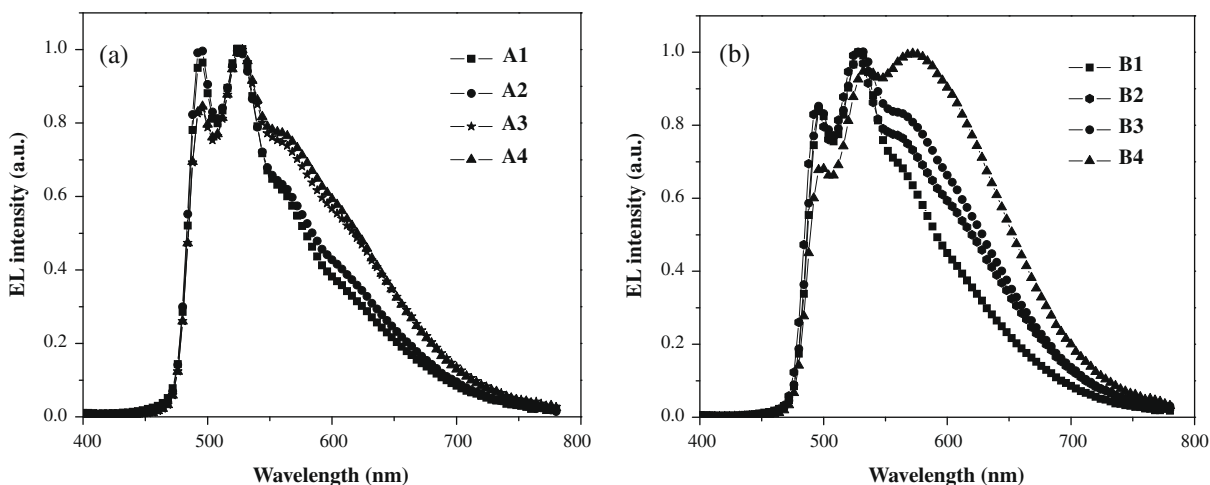


Fig. 9. EL spectra of (a) **2** and (b) **3**-doped OLEDs at different dopant concentrations.

tions. Such characteristics have been used in the literature to fabricate white OLEDs by using excimer or aggregate emission from a phosphor dopant coupled with the blue emission from the host due to the incomplete energy transfer [83,85–88].

Although all of the devices show monomer and red-shifted excimer or aggregate emissions, the intensity of the peaks clearly vary. Whether the occurrence of this low-energy emission is due to excimer or aggregation formation certainly needs more investigation. Device **B5** shows the Commission Internationale de L'Eclairage (CIE) value  $x = 0.25$ ,  $y = 0.45$  which appears near white to the naked eyes. The green OLEDs utilizing compounds **2** and **3** have CIE coordinates of (0.34, 0.55) and (0.36, 0.56), respectively at 3 wt.-%. The electrical characteristics of these devices are displayed in the current density–voltage–luminance ( $J$ – $V$ – $L$ ) curves (Fig. 10). From the data, the current density decreases as the doping concentration increases at the same driving potential. This is mainly attributed to the increased amount of hole trapping when the platinum molecules tend to aggregate upon device operation at a higher doping concentration. The overall efficiencies of the device **B3** appear the highest among the green-emitting devices in this study. It has a turn-on voltage of 7.7 V, maximum luminance of 2271 cd/m<sup>2</sup> at 13.5 V, external quantum efficiency ( $\eta_{\text{ext}}$ ) of 1.23%, power efficiency ( $\eta_{\text{p}}$ ) of 0.77 lm/W and current efficiency ( $\eta_{\text{L}}$ ) of 2.80 cd/A, respectively. On the contrary, for complex **2** at the same doping

concentration (device **A3**), it shows a poorer performance with  $\eta_{\text{ext}}$  of 0.28%,  $\eta_{\text{p}}$  of 0.18 lm/W and  $\eta_{\text{L}}$  of 0.77 cd/A. We notice a rather slow drop of the EL efficiency with increasing voltage. This may be attributed to the relatively short lifetimes of these complexes that can help to reduce the roll-off resulting from electric field-induced exciton quenching effects, exciton–exciton annihilation, and charge–carrier–exciton interactions on long-lived excited states, as found for other electrophosphorescent devices [89,90].

To illustrate the difference of substituents on the pyridyl ring in the device efficiencies, compound **4** was also fabricated in the same configuration. The device displays an intense green-yellow emission with a peak maximum and a shoulder at around 516 nm and 544 nm, respectively, in the EL spectrum with CIE coordinates (0.34, 0.61) for device **C2**, which closely resembles the PL spectrum in dichloromethane solution, indicating that the EL emission of the device originates from the triplet excited states of the phosphor. Fig. 11 displays the EL spectra of **4**-doped OLEDs. The EL spectra changed slightly with the doping concentration due to excimer formation. Relative to the non-trifluoromethylated complexes **2** and **3**, the emission caused by aggregation or  $\pi$ – $\pi$  stacking is significantly weaker for **4** especially at high doping concentrations. This may be attributed to the introduction of sterically bulky CF<sub>3</sub> group which can alter the molecular packing and minimize the self-quenching behavior [69,91–93].

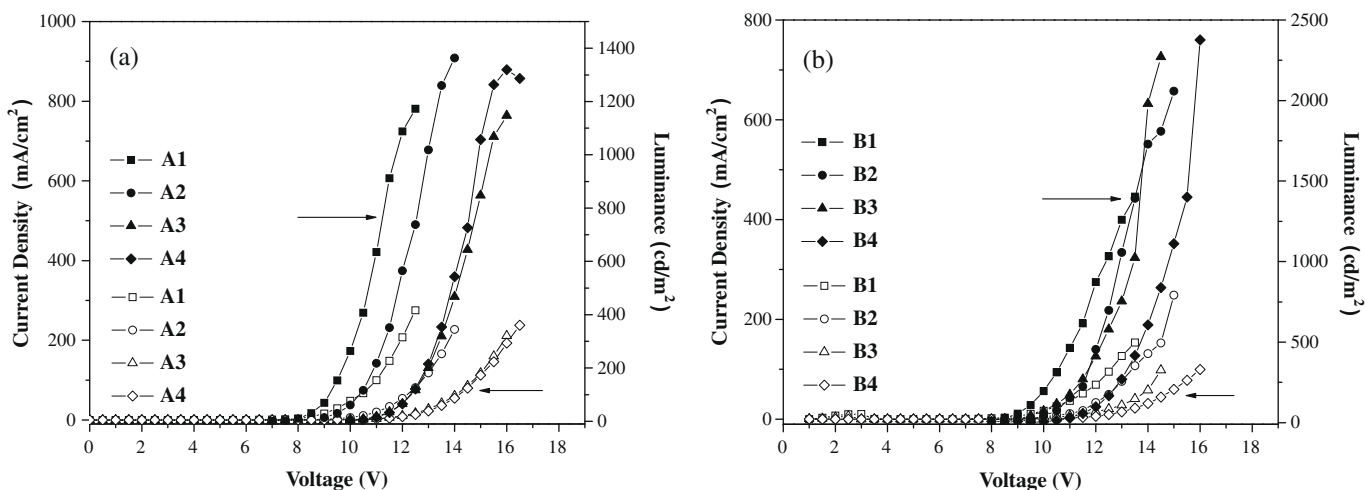


Fig. 10. Current density–voltage–luminance ( $J$ – $V$ – $L$ ) characteristics of the electrophosphorescent OLED devices with different dopant levels of (a) **2** and (b) **3**.

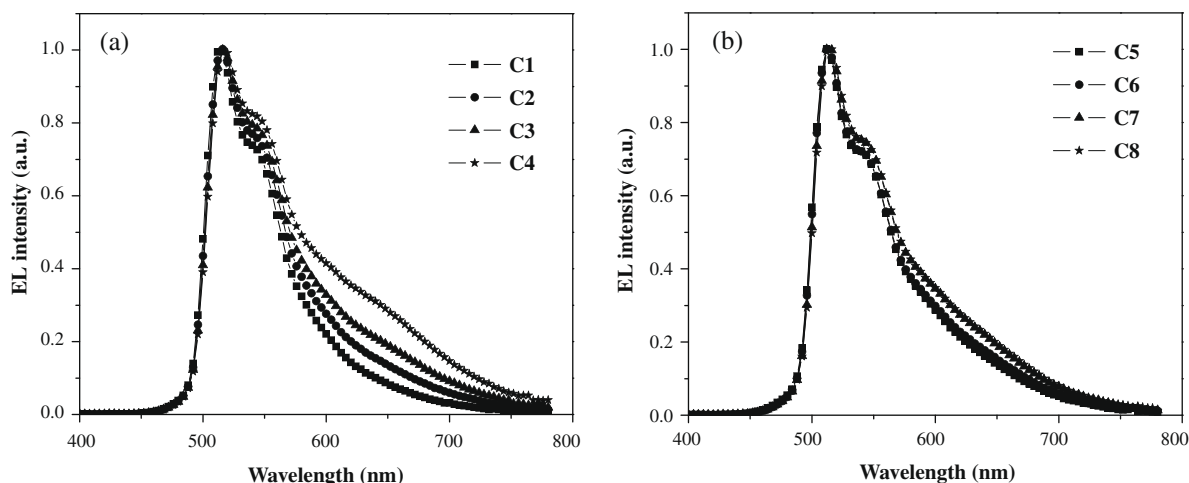


Fig. 11. EL spectra of **4**-doped OLEDs prepared from (a)  $\text{CHCl}_3$  and (b) toluene at different dopant concentrations.

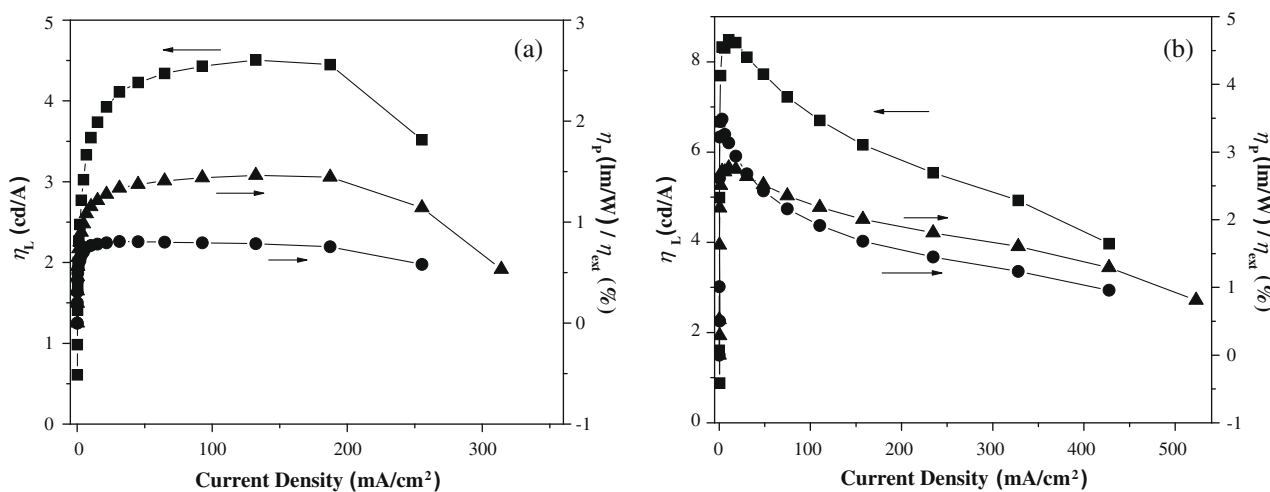


Fig. 12.  $\eta_L$  (■),  $\eta_P$  (●) and  $\eta_{\text{ext}}$  (▲) as a function of current density for OLED devices (a) **C3** and (b) **C7**.

Significantly better performance and lower turn-on voltage were achieved for **4** under the same doping level, especially in the case of using toluene as solvent for the spin-coating process. This may be due to the higher solubility effect by the  $\text{CF}_3$  group which can facilitate the homogeneous film formation as compared to the unsubstituted one. The lower turn-on voltage is presumably caused by the reduced electron injection barrier after introduction of the trifluoromethyl substituents, that is in agreement with the lower LUMO level estimated from the results of cyclic voltammetry and literature reports in which fluorination is expected to enhance the electron mobility, reduce triplet-triplet annihilation processes [59,94] and result in a better balance of charge injection. The markedly higher luminance efficiency and brightness were achieved at the 6 and 9 wt.-% doping concentrations (devices **C6** and **C7**). For device **C7**, the maximum luminance is  $16960 \text{ cd/m}^2$  at 13 V. The maximum  $\eta_L$ ,  $\eta_{\text{ext}}$  and  $\eta_P$  are 8.49 cd/A, 2.77% and 3.48 lm/W, respectively. For device **C6**, the EL data are characterized by a maximum brightness of  $16150 \text{ cd/m}^2$  at 12.5 V, and peak efficiencies of 8.33 cd/A, 2.65% and 3.89 lm/W, respectively. We note that the  $\eta_L$ ,  $\eta_P$  and  $\eta_{\text{ext}}$  decrease by a larger extent for devices spin-coated with toluene but such decrease is not apparent for devices spin-coated with chloroform up to  $200 \text{ mA/cm}^2$  at the same doping concentrations. Fig. 12 shows the  $\eta_L$ ,  $\eta_{\text{ext}}$  and  $\eta_P$  data as a function of current density for OLED devices **C3** and **C7**.

The observation of different EL performance by using  $\text{CHCl}_3$  and toluene as the processing solvents suggest that the relative inten-

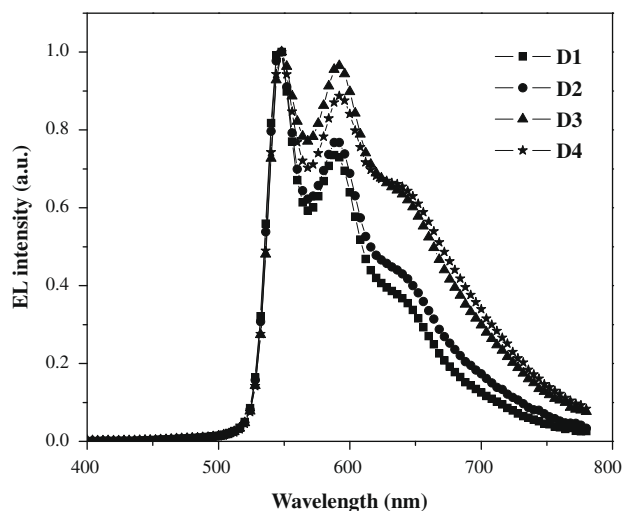


Fig. 13. EL spectra of **8**-doped OLEDs at different dopant concentrations.

sities of monomer and excimer emission are dependent of the nature of solvent used as well as the doping level. At the same doping concentration, degree of aggregation by dopant packing was dissimilar in the two solvent systems. Diminished aggregation arising from the excimer formation was observed by using toluene and accordingly, toluene-coated devices gave a higher luminance at the same voltage.

The devices derived from **8** were also fabricated. Fig. 13 shows the normalized EL spectra of devices doped with **8** in different doping concentrations. Similar to other complexes, a concentration dependent EL spectra was observed. Each of them emits an orange color centered at 548 nm with a broad shoulder at around 640 nm. As the concentration was increased, it revealed a clear aggregation phenomenon. The CIE coordinates of **8** are (0.49, 0.51) at 6 wt.-% doping concentration. A maximum  $\eta_{\text{ext}}$  of 0.40%,  $\eta_{\text{p}}$  of 0.19 lm/W and  $\eta_{\text{l}}$  of 1.13 cd/A was achieved for complex **8** at 3 wt.-% doping. The device performance only slightly decreases with increasing current density and remains as  $\eta_{\text{ext}} = 0.39\%$ ,  $\eta_{\text{p}} = 0.19$  lm/W and  $\eta_{\text{l}} = 1.12$  cd/A at a luminance of 1000 cd/m<sup>2</sup>. The luminance reaches a maximum of 1592 cd/m<sup>2</sup> at 19.5 V at this concentration.

### 3. Concluding remarks

In summary, a series of luminescent Pt(II) complexes featuring functionalized hole-transporting carbazole ligands were synthesized. The structure–property–function relationships of the resulting Pt(II) complexes were studied as a function of ligand and substituent effects. A variety of cyclometalating ligands can be used to tune the energy of the emissive state over a wide spectral color range. Strong spin–orbit coupling of the heavy Pt atom allows for mixing of <sup>1</sup>MLCT with ligand-based <sup>3</sup> $\pi$ – $\pi$  states, making the formally forbidden radiative relaxation of these states an efficient process, therefore all of these complexes exhibit intense phosphorescence emissions at room temperature. These neutral and air-stable complexes are easily prepared, rendering them good potential as candidates for use in optoelectronics devices. We have also incorporated some of these Pt complexes into OLEDs based on solution-processing method. While the device performance is yet to be optimized, extension of these carbazole derivatives to other device configurations or by vacuum deposition would warrant further investigation.

## 4. Experimental

### 4.1. General information

All reactions were performed under nitrogen. Solvents were carefully dried and distilled from appropriate drying agents prior to use. Commercially available reagents were used without further purification unless otherwise stated. All reactions were monitored by thin-layer chromatography (TLC) with Merck pre-coated glass plates. Flash column chromatography and preparative TLC were carried out using silica gel from Merck (230–400 mesh). Fast atom bombardment (FAB) mass spectra were recorded on a Finnigan MAT SSQ710 system. NMR spectra were measured in CDCl<sub>3</sub> on a Varian Inova 400 MHz FT-NMR spectrometer; chemical shifts were quoted relative to the internal standard tetramethylsilane for <sup>1</sup>H and <sup>13</sup>C{<sup>1</sup>H} NMR data.

### 4.2. General procedures for the synthesis of cyclometalated platinum(II) complexes

The ligands **L**<sub>1</sub>–**L**<sub>10</sub> were prepared following the published procedures [37–42].

All of the cyclometalated platinum(II) complexes were synthesized by refluxing a mixture of 2.5 molar equivalents of the corresponding ligand and K<sub>2</sub>PtCl<sub>4</sub> in a mixture of 2-ethoxyethanol and water (3:1, v/v) under a nitrogen atmosphere to 80 °C for 16 h. After cooling to room temperature, the mixture was added to water (20 mL), and the precipitate was washed with water (20 mL × 4) and dried at 50 °C under vacuum. Without further purification, the precipitate was then treated with 3 molar equivalents of acetylacetone and 10 equivalents of Na<sub>2</sub>CO<sub>3</sub> in 2-ethoxyethanol (8 mL) at 100 °C under nitrogen for 16 h. After the removal of all volatile components, the compound was purified by column chromatography on silica using CH<sub>2</sub>Cl<sub>2</sub>/hexane mixture as the eluent to afford the desired products.

**1:** A pale yellow powder (yield: 16%). MS (FAB): *m/z* 613 (M<sup>+</sup>). <sup>1</sup>H NMR (CDCl<sub>3</sub>):  $\delta$  (ppm) 8.95 (d, 1H, *J* = 5.4 Hz, Ar), 8.22 (s, 1H, Ar), 8.10 (d, 1H, *J* = 8.1 Hz, Ar), 7.78 (m, 2H, Ar), 7.66–7.55 (m, 6H, Ar), 7.45–7.25 (m, 3H, Ar), 7.05 (m, 1H, Ar), 5.43 (s, 1H, acac), 2.04 (s, 3H, CH<sub>3</sub>), 1.88 (s, 3H, CH<sub>3</sub>). Anal. Calc. for C<sub>28</sub>H<sub>22</sub>N<sub>2</sub>O<sub>2</sub>Pt: C, 54.81; H, 3.61; N, 4.57. Found: C, 54.65; H, 3.44; N, 4.67%.

**2:** A pale yellow powder (yield: 18%). MS (FAB): *m/z* 631 (M<sup>+</sup>). <sup>1</sup>H NMR (CDCl<sub>3</sub>):  $\delta$  (ppm) 8.96 (m, 1H, Ar), 8.22 (s, 1H, Ar), 8.10 (d, 1H, *J* = 8.1 Hz, Ar), 7.78 (m, 2H, Ar), 7.63–7.58 (m, 2H, Ar), 7.37–7.25 (m, 6H, Ar), 7.04 (m, 1H, Ar), 5.44 (s, 1H, acac), 1.99–1.89 (m, 6H, CH<sub>3</sub>). Anal. Calc. for C<sub>28</sub>H<sub>21</sub>N<sub>2</sub>FO<sub>2</sub>Pt: C, 53.25; H, 3.35; N, 4.44. Found: C, 53.43; H, 3.53; N, 4.55%.

**3:** A pale yellow powder (yield: 31%). MS (FAB): *m/z* 643 (M<sup>+</sup>). <sup>1</sup>H NMR (CDCl<sub>3</sub>):  $\delta$  (ppm) 8.94 (d, 1H, *J* = 2.7 Hz, Ar), 8.20 (s, 1H, Ar), 8.09 (d, 1H, *J* = 8.1 Hz, Ar), 7.76 (m, 2H, Ar), 7.55–7.07 (m, 9H, Ar), 5.43 (s, 1H, acac), 3.90 (s, 3H, OMe), 1.98 (s, 3H, CH<sub>3</sub>), 1.88 (s, 3H, CH<sub>3</sub>). <sup>13</sup>C NMR (CDCl<sub>3</sub>):  $\delta$  (ppm) 185.49, 183.76 (CO), 183.76, 168.52, 158.49, 146.85, 142.11, 141.01, 137.80, 136.85, 136.73, 130.30, 128.48, 124.85, 124.15, 119.81, 119.56, 119.15, 117.73, 115.65, 114.60, 110.32, 109.86 (Ar), 102.36 (CH), 55.64 (OMe), 28.35, 27.22 (CH<sub>3</sub>). Anal. Calc. for C<sub>29</sub>H<sub>24</sub>N<sub>2</sub>O<sub>3</sub>Pt: C, 54.12; H, 3.76; N, 4.35. Found: C, 53.89; H, 3.82; N, 4.49%.

**4:** A yellow powder (yield: 28%). MS (FAB): *m/z* 681 (M<sup>+</sup>). <sup>1</sup>H NMR (CDCl<sub>3</sub>):  $\delta$  (ppm) 9.14 (s, 1H, Ar), 8.15 (s, 1H, Ar), 8.01 (d, 1H, *J* = 5.4 Hz, Ar), 7.86 (d, 1H, *J* = 5.4 Hz, Ar), 7.73 (d, 1H, *J* = 5.4 Hz, Ar), 7.54–7.18 (m, 9H, Ar), 5.38 (s, 1H, acac), 1.94 (s, 3H, CH<sub>3</sub>), 1.82 (s, 3H, CH<sub>3</sub>). <sup>13</sup>C NMR (CDCl<sub>3</sub>):  $\delta$  (ppm) 186.13, 184.00 (CO), 144.30, 142.67, 140.85, 138.58, 137.35, 135.19, 134.67, 129.54, 127.48, 127.19, 125.41, 124.28, 122.85, 122.50, 120.49, 120.16, 119.38, 117.48, 117.35, 110.56, 110.21 (Ar), 102.55 (CH), 28.28, 26.98 (CH<sub>3</sub>), 14.12 (CF<sub>3</sub>). Anal. Calc. for C<sub>29</sub>H<sub>21</sub>N<sub>2</sub>F<sub>3</sub>O<sub>2</sub>Pt: C, 51.11; H, 3.11; N, 4.11. Found: C, 51.32; H, 3.02; N, 4.13%.

**5:** A pale yellow powder (yield: 69%). MS (FAB): *m/z* 631 (M<sup>+</sup>). <sup>1</sup>H NMR (CDCl<sub>3</sub>):  $\delta$  (ppm) 8.90 (m, 1H, Ar), 8.15–8.08 (m, 2H, Ar), 7.78–7.36 (m, 11H, Ar), 5.44 (s, 1H, acac), 2.00 (s, 3H, Me), 1.88 (s, 3H, CH<sub>3</sub>). Anal. Calc. for C<sub>28</sub>H<sub>21</sub>N<sub>2</sub>FO<sub>2</sub>Pt: C, 53.25; H, 3.35; N, 4.44. Found: C, 53.10; H, 3.30; N, 4.57%.

**6:** A yellow powder (yield: 29%). MS (FAB): *m/z* 627 (M<sup>+</sup>). <sup>1</sup>H NMR (CDCl<sub>3</sub>):  $\delta$  (ppm) 8.70–8.69 (d, 1H, *J* = 2.7 Hz, Ar), 8.17 (s, 1H, Ar), 8.08 (d, 1H, *J* = 5.4 Hz, Ar), 7.65–7.54 (m, 6H, Ar), 7.43–7.34 (m, 3H, Ar), 6.81 (m, 1H, Ar), 6.80 (m, 1H, Ar), 5.40 (s, 1H, acac), 2.41 (s, 3H, CH<sub>3</sub>), 1.95 (s, 3H, CH<sub>3</sub>), 1.85 (s, 3H, CH<sub>3</sub>). <sup>13</sup>C NMR (CDCl<sub>3</sub>):  $\delta$  (ppm) 185.56, 183.79 (CO), 167.83, 149.65, 146.20, 141.62, 140.59, 137.72, 137.21, 137.00, 129.42, 127.17, 127.13, 124.90, 121.15, 120.02, 119.73, 119.25, 118.50, 115.37, 110.33, 109.94 (Ar), 102.35 (CH), 28.25, 27.04 (CH<sub>3</sub>), 21.57 (CH<sub>3</sub>). Anal. Calc. for C<sub>29</sub>H<sub>24</sub>N<sub>2</sub>O<sub>2</sub>Pt: C, 55.50; H, 3.85; N, 4.46. Found: C, 55.43; H, 3.76; N, 4.48%.

**7:** A yellow powder (yield: 54%). MS (FAB): *m/z* 613 (M<sup>+</sup>). <sup>1</sup>H NMR (CDCl<sub>3</sub>):  $\delta$  (ppm) 9.04–9.02 (d, 1H, *J* = 5.4 Hz, Ar), 8.13 (d, 2H, *J* = 2.7 Hz, Ar), 7.87–7.68 (m, 2H, Ar), 7.68–7.62 (m, 2H, Ar), 7.56 (m, 2H, Ar), 7.41–7.31 (m, 2H, Ar), 7.28 (m, 3H, Ar), 7.16 (m,

**Table 6**  
Summary of crystal data.

	1	2	3	4	8	9	10
CCDC no.	717476	717477	717478	717479	717480	717481	717482
Formula	C <sub>28</sub> H <sub>22</sub> N <sub>2</sub> O <sub>2</sub> Pt	C <sub>28</sub> H <sub>21</sub> N <sub>2</sub> FO <sub>2</sub> Pt	C <sub>29</sub> H <sub>24</sub> N <sub>2</sub> O <sub>3</sub> Pt	C <sub>29</sub> H <sub>21</sub> N <sub>2</sub> F <sub>3</sub> O <sub>2</sub> Pt	C <sub>39</sub> H <sub>34</sub> N <sub>2</sub> O <sub>2</sub> Pt·2H <sub>2</sub> O	C <sub>32</sub> H <sub>24</sub> N <sub>2</sub> O <sub>2</sub> Pt	C <sub>33</sub> H <sub>26</sub> N <sub>2</sub> O <sub>3</sub> Pt
<i>M<sub>r</sub></i>	613.57	631.56	643.59	681.57	793.80	663.62	693.65
Crystal size (mm)	0.28 × 0.25 × 0.15	0.30 × 0.13 × 0.11	0.23 × 0.21 × 0.20	0.28 × 0.26 × 0.26	0.30 × 0.25 × 0.22	0.29 × 0.23 × 0.15	0.31 × 0.24 × 0.14
Crystal system	Triclinic	Triclinic	Triclinic	Monoclinic	Monoclinic	Monoclinic	Triclinic
Space group	<i>P</i> $\bar{1}$	<i>P</i> $\bar{1}$	<i>P</i> $\bar{1}$	<i>P</i> <sub>2</sub> / <i>c</i>	<i>P</i> <sub>2</sub> / <i>n</i>	<i>P</i> <sub>2</sub> / <i>c</i>	<i>P</i> $\bar{1}$
<i>a</i> (Å)	7.1749(5)	7.1661(8)	7.0782(4)	13.1924(7)	15.1757(7)	11.6935(6)	10.895(1)
<i>b</i> (Å)	11.4511(9)	11.537(1)	11.6085(7)	11.9666(6)	12.8628(6)	8.6213(4)	13.886(2)
<i>c</i> (Å)	13.557(1)	13.693(2)	14.9566(9)	32.939(2)	17.5829(8)	25.188(1)	20.094(2)
$\alpha$ (°)	94.376(1)	95.622(2)	101.067(1)	90	90	90	72.831(2)
$\beta$ (°)	98.620(1)	98.124(2)	96.455(1)	99.006(1)	94.843(1)	94.267(1)	80.262(2)
$\gamma$ (°)	94.054(1)	94.740(2)	95.303(1)	90	90	90	69.524(2)
<i>V</i> (Å <sup>3</sup> )	1094.2(1)	1110.0(2)	1190.2(1)	5135.9(5)	3420.0(3)	2532.3(2)	2713.6(5)
<i>Z</i>	2	2	2	8	4	4	4
<i>D</i> <sub>calcd</sub> (g cm <sup>-3</sup> )	1.862	1.890	1.796	1.763	1.542	1.741	1.698
$\mu$ (mm <sup>-1</sup> )	6.441	6.359	5.929	5.515	4.145	5.574	5.208
<i>F</i> (000)	596	612	628	2640	1584	1296	1360
$\theta$ range (°)	1.79–25.00	2.21–25.00	1.80–28.27	1.81–25.00	1.96–25.00	2.29–25.00	2.00–25.00
No. of reflections collected	5438	5567	7063	25 175	16 621	12 065	13 293
No. of unique reflections	3779	3852	5179	9039	5994	4448	9345
[ <i>R</i> <sub>int</sub> ]	0.0244	0.0286	0.0262	0.0313	0.0284	0.0349	0.0400
No. of reflections with <i>I</i> > 2.0 $\sigma$ ( <i>I</i> )	3488	3252	4794	6614	4620	3757	5766
No. of parameters	298	307	316	667	415	334	703
<i>R</i> <sub>1</sub> [ <i>I</i> > 2.0 $\sigma$ ( <i>I</i> )] <sup>a</sup>	0.0324	0.0345	0.0291	0.0294	0.0271	0.0254	0.0523
<i>wR</i> <sub>2</sub> (all data) <sup>a</sup>	0.0844	0.0773	0.0766	0.0748	0.0719	0.0639	0.1323
GOF on <i>F</i> <sup>2b</sup>	1.060	1.003	1.023	1.028	1.045	1.001	0.983

<sup>a</sup>  $R_1 = \sum ||F_o| - |F_c|| / \sum |F_o|$ .  $wR_2 = \{ \sum [w(F_o^2 - F_c^2)^2] / \sum [w(F_o^2)^2] \}^{1/2}$ .

<sup>b</sup>  $GOF = \{ (\sum [w(F_o^2 - F_c^2)^2] / (N_{obs} - N_{param})) \}^{1/2}$ .

1H, Ar), 5.44 (s, 1H, acac), 2.00 (s, 3H, CH<sub>3</sub>), 1.84 (s, 3H, CH<sub>3</sub>). <sup>13</sup>C NMR (CDCl<sub>3</sub>):  $\delta$  (ppm) 185.85, 184.44 (CO), 167.45, 147.48, 143.76, 140.89, 138.36, 137.80, 128.61, 125.79, 124.09, 123.33, 122.05, 121.44, 120.08, 119.65, 118.65, 110.46 (Ar), 102.58 (CH), 28.20, 27.05 (CH<sub>3</sub>). Anal. Calc. for C<sub>28</sub>H<sub>22</sub>N<sub>2</sub>O<sub>2</sub>Pt: C, 54.81; H, 3.61; N, 4.57. Found: C, 54.76; H, 3.54; N, 4.75%.

**8:** An orange powder (yield: 37%). MS (FAB): *m/z* 757 (M<sup>+</sup>). <sup>1</sup>H NMR (CDCl<sub>3</sub>):  $\delta$  (ppm) 9.02–9.01 (d, 1H, *J* = 2.7 Hz, Ar), 8.18–7.99 (m, 4H, Ar), 7.99–7.70 (m, 2H, Ar), 7.54–7.29 (m, 9H, Ar), 7.08 (m, 1H, Ar), 5.51 (s, 1H, acac), 2.09–2.03 (m, 10H, C<sub>2</sub>H<sub>5</sub> + CH<sub>3</sub>), 0.46 (t, 6H, *J* = 13.5 Hz, C<sub>2</sub>H<sub>5</sub>). <sup>13</sup>C NMR (CDCl<sub>3</sub>):  $\delta$  (ppm) 185.85, 184.10 (CO), 184.10, 168.17, 152.45, 147.27, 145.59, 143.71, 142.06, 141.08, 141.04, 138.00, 137.80, 136.35, 125.90, 125.71, 123.26, 121.51, 121.45, 120.83, 120.28, 119.74, 118.39, 117.49, 109.83 (Ar), 102.61 (CH), 56.01 (quat. C), 28.31, 27.23 (CH<sub>3</sub>), 32.98, 8.65 (C<sub>2</sub>H<sub>5</sub>). Anal. Calc. for C<sub>39</sub>H<sub>34</sub>N<sub>2</sub>O<sub>2</sub>Pt: C, 61.82; H, 4.52; N, 3.70. Found: C, 61.70; H, 4.34; N, 3.91%.

**9:** A red powder (yield: 12%). MS (FAB): *m/z* 663 (M<sup>+</sup>). <sup>1</sup>H NMR (CDCl<sub>3</sub>):  $\delta$  (ppm) 9.13 (m, 1H, Ar), 8.97–8.91 (m, 2H, Ar), 8.26 (d, 1H, *J* = 8.1 Hz, Ar), 7.90–7.65 (m, 9H, Ar), 7.55–7.33 (m, 4H, Ar), 5.52 (s, 1H, acac), 2.09 (s, 3H, CH<sub>3</sub>), 1.97 (s, 3H, CH<sub>3</sub>). <sup>13</sup>C NMR (CDCl<sub>3</sub>):  $\delta$  (ppm) 185.75, 183.81 (CO), 171.89, 141.47, 140.54, 139.60, 138.99, 138.23, 137.44, 137.38, 130.90, 129.39, 128.06, 127.36, 127.17, 127.00, 126.55, 125.55, 124.94, 124.84, 121.42, 120.26, 119.59, 119.14, 118.14, 110.47, 109.11 (Ar), 102.38 (CH), 55.61 (OMe), 28.43 (CH<sub>3</sub>). Anal. Calc. for C<sub>32</sub>H<sub>24</sub>N<sub>2</sub>O<sub>2</sub>Pt: C, 57.92; H, 3.65; N, 4.22. Found: C, 57.87; H, 3.55; N, 4.12%.

**10:** A red powder (yield: 11%). MS (FAB): *m/z* 693 (M<sup>+</sup>). <sup>1</sup>H NMR (CDCl<sub>3</sub>):  $\delta$  (ppm) 9.02–9.01 (d, 1H, *J* = 2.7 Hz, Ar), 8.83–8.76 (m, 2H, Ar), 8.11 (d, 1H, *J* = 8.1 Hz, Ar), 7.77–7.68 (m, 3H, Ar), 7.58–7.48 (m, 3H, Ar), 7.31–7.28 (m, 4H, Ar), 7.05 (d, 2H, *J* = 8.1 Hz, Ar), 5.38 (s, 1H, acac), 3.85 (s, 3H, OMe), 1.95 (s, 3H, CH<sub>3</sub>), 1.83 (s, 3H, CH<sub>3</sub>). <sup>13</sup>C NMR (CDCl<sub>3</sub>):  $\delta$  (ppm) 185.92, 184.04 (CO), 169.61, 158.66, 141.99, 141.09, 139.54, 139.07, 138.09,

137.49, 131.02, 130.22, 128.45, 128.16, 127.44, 126.70, 125.60, 124.96, 124.68, 121.56, 120.11, 119.47, 119.16, 118.15, 114.67, 110.46, 110.09 (Ar), 102.44 (CH), 55.61 (OMe), 28.35, 27.17 (CH<sub>3</sub>). Anal. Calc. for C<sub>33</sub>H<sub>26</sub>N<sub>2</sub>O<sub>3</sub>Pt: C, 57.14; H, 3.78; N, 4.04. Found: C, 57.01; H, 3.93; N, 3.94%.

## 5. X-ray crystallography

Crystals suitable for X-ray diffraction studies were grown by slow evaporation of each of the respective solutions in CH<sub>2</sub>Cl<sub>2</sub>/hexane at room temperature. Geometric and intensity data were collected at 293 K using graphite-monochromated Mo K $\alpha$  radiation ( $\lambda$  = 0.71073 Å) on a Bruker Axs SMART 1000 CCD diffractometer. The collected frames were processed with the software SAINT [95] and an absorption correction (SADABS) [96] was applied to the collected reflections. The structure was solved by the Direct or Patterson methods (SHELXL) [97] in conjunction with standard difference Fourier techniques and subsequently refined by full-matrix least-squares analyses on *F*<sup>2</sup>. Hydrogen atoms were generated in their idealized positions and all non-hydrogen atoms were assigned with anisotropic displacement parameters. Pertinent crystal data for the structures are collected in Table 6.

## Acknowledgements

This work was supported by a CERG Grant from the Hong Kong Research Grants Council (HKBU202005) and a Faculty Research Grant from the Hong Kong Baptist University (FRG/08-09/1-20).

## Appendix A. Supplementary material

CCDC 717476, 717477, 717478, 717479, 717480, 717481 and 717482 contain the supplementary crystallographic data for this

paper. These data can be obtained free of charge from The Cambridge Crystallographic Data Centre via [www.ccdc.cam.ac.uk/data\\_request/cif](http://www.ccdc.cam.ac.uk/data_request/cif). Supplementary data associated with this article can be found, in the online version, at [doi:10.1016/j.jorganchem.2009.03.002](https://doi.org/10.1016/j.jorganchem.2009.03.002).

## References

- [1] A.S. Ionkin, W.J. Marshall, Y. Wang, *Organometallics* 24 (2005) 619.
- [2] S.C. Chan, M.C.W. Chan, Y. Wang, C.M. Che, K.K. Cheung, N. Zhu, *Chem. Eur. J.* (2001) 4180.
- [3] E.A.M. Geary, L.J. Yellowlees, L.A. Jack, I.D.H. Oswald, S. Parsons, N. Hirata, J.R. Durrant, N. Roberson, *Inorg. Chem.* 44 (2005) 242.
- [4] P.K.M. Siu, D.L. Ma, C.M. Che, *Chem. Commun.* (2005) 1025.
- [5] G. Hughes, M.R. Bryce, *J. Mater. Chem.* 25 (2005) 94.
- [6] J. Brooks, Y. Babayan, S. Lamansky, P.I. Djurovich, I. Tsyba, R. Bau, M.E. Thompson, *Inorg. Chem.* 41 (2002) 3055.
- [7] J.A.G. Williams, S. Develay, D.L. Rochester, L. Murphy, *Coord. Chem. Rev.* 252 (2008) 2596.
- [8] W.-Y. Wong, *Dalton Trans.* (2007) 4495.
- [9] W.-Y. Wong, *J. Inorg. Organomet. Polym. Mater.* 15 (2005) 197.
- [10] W.-Y. Wong, C.-L. Ho, *Coord. Chem. Rev.* 250 (2006) 2627.
- [11] J.A. Zuleta, J.M. Bevilacqua, R. Eisenberg, *Coord. Chem. Rev.* 111 (1992) 237.
- [12] C.W. Chan, L.K. Cheng, C.M. Che, *Coord. Chem. Rev.* 132 (1994) 87.
- [13] S.D. Cummings, R. Eisenberg, *Prog. Inorg. Chem.* 32 (2003) 315.
- [14] T.J. Wadas, R.J. Lachicotte, R. Eisenberg, *Inorg. Chem.* 42 (2003) 3772.
- [15] M. Hissler, W.B. Connick, D.K. Geiger, J.E. McGarrah, D. Lipa, R.J. Lachicotte, R. Eisenberg, *Inorg. Chem.* 39 (2000) 447.
- [16] W. Paw, S.D. Cummings, M.A. Mansour, W.B. Connick, D.K. Geiger, R. Eisenberg, *Coord. Chem. Rev.* 171 (1998) 125.
- [17] S.D. Cummings, R. Eisenberg, *J. Am. Chem. Soc.* 118 (1996) 1949.
- [18] S.D. Cummings, R. Eisenberg, *Inorg. Chem.* 34 (1995) 2007.
- [19] J.M. Bevilacqua, R. Eisenberg, *Inorg. Chem.* 33 (1994) 1886.
- [20] J.M. Bevilacqua, J.A. Zuleta, R. Eisenberg, *Inorg. Chem.* 33 (1994) 258.
- [21] J.A. Zuleta, M.S. Burberry, R. Eisenberg, *Coord. Chem. Rev.* 97 (1990) 47.
- [22] J.A. Zuleta, J.M. Bevilacqua, R.M. Rehm, R. Eisenberg, *Inorg. Chem.* 31 (1992) 1332.
- [23] J.A. Zuleta, J.M. Bevilacqua, D.M. Proserpio, P.D. Harvey, R. Eisenberg, *Inorg. Chem.* 31 (1992) 2396.
- [24] P. Shao, Y. Li, W. Sun, *J. Phys. Chem. A* 112 (2008) 1172.
- [25] B. Yin, F. Niemeyer, J.A.G. Williams, J. Jiang, A. Boucekine, L. Toupet, H.L. Bozec, V. Guerschais, *Inorg. Chem.* 45 (2006) 8584.
- [26] H. Yersin, D. Donges, H. Humbs, J. Strasser, *Inorg. Chem.* 41 (2002) 4915.
- [27] P. Jolliet, M. Gianini, A. von Zelewsky, G. Bernardinelli, H. Stoeckli-Evans, *Inorg. Chem.* 35 (1996) 4883.
- [28] C.H. Chen, J. Shi, C.W. Tang, *Coord. Chem. Rev.* 171 (1998) 161.
- [29] S. Tokito, H. Tanaka, K. Noda, A. Okada, T. Taga, *Appl. Phys. Lett.* 70 (1997) 1929.
- [30] Y. Kuwabara, H. Ogawa, H. Inada, N. Noma, Y. Shirota, *Adv. Mater.* 6 (1994) 677.
- [31] D.F. O'Brien, P.E. Burrows, S.R. Forrest, B.E. Koene, D.E. Loy, M.E. Thompson, *Adv. Mater.* 10 (1998) 1108.
- [32] W.-Y. Wong, *Coord. Chem. Rev.* 249 (2005) 971.
- [33] P.I. Kvam, M.V. Puzyk, K.P. Balashev, J. Songstad, *Acta Chem. Scand.* 49 (1995) 335.
- [34] K.P. Balashev, M.V. Puzyk, V.S. Kotlyar, M.V. Kulikova, *Coord. Chem. Rev.* 159 (1997) 109.
- [35] W.-Y. Wong, Z. He, S.-K. So, K.-L. Tong, Z. Lin, *Organometallics* 24 (2005) 4097.
- [36] Z. He, W.-Y. Wong, X. Yu, H.-S. Kwok, Z. Lin, *Inorg. Chem.* 45 (2006) 10922.
- [37] W.-Y. Wong, C.-L. Ho, Z.-Q. Gao, B.-X. Mi, C.-H. Chen, K.-W. Cheah, Z. Lin, *Angew. Chem., Int. Ed.* 45 (2006) 7800.
- [38] C.-L. Ho, W.-Y. Wong, G.-J. Zhou, B. Yao, Z. Xie, L. Wang, *Adv. Funct. Mater.* 17 (2007) 2925.
- [39] C.-L. Ho, Q. Wang, C.-S. Lam, W.-Y. Wong, D. Ma, L. Wang, Z.-Q. Gao, C.-H. Chen, K.-W. Cheah, Z. Lin, *Chem. Asian J.* 4 (2009) 89.
- [40] C.-L. Ho, W.-Y. Wong, Z.-Q. Gao, C.-H. Chen, K.-W. Cheah, B. Yao, Z. Xie, Q. Wang, D. Ma, L. Wang, X.-M. Yu, H.-S. Kwok, Z. Lin, *Adv. Funct. Mater.* 18 (2008) 319.
- [41] C.-L. Ho, M.-F. Lin, W.-Y. Wong, W.-K. Wong, C.-H. Chen, *Appl. Phys. Lett.* 92 (2008) 083301.
- [42] C.-L. Ho, W.-Y. Wong, Q. Wang, D. Ma, L. Wang, Z. Lin, *Adv. Funct. Mater.* 18 (2008) 928.
- [43] C. Bolm, M. Ewald, M. Felder, G. Schingloff, *Chem. Ber.* 125 (1992) 1169.
- [44] N. Miyaura, A. Suzuki, *Chem. Rev.* 95 (1995) 2457.
- [45] P.I. Shih, C.F. Shu, Y.L. Tung, Y. Chi, *Appl. Phys. Lett.* 88 (2006) 251110.
- [46] R. Anémian, J.C. Mulatier, C. Andraud, O. Stéphan, J.C. Vial, *Chem. Commun.* (2002) 1608.
- [47] O. Lohse, P. Thevenin, E. Waldvogel, *Synlett* 1 (1999) 45.
- [48] K. Brunner, A. van Dijken, H. Börner, J.J.A.M. Bastiaansen, N.M.M. Kiggen, B.M.W. Langeveld, *J. Am. Chem. Soc.* 126 (2004) 6035.
- [49] O. Paliulis, J. Ostrauskaite, V. Gaidelis, V. Jankauskas, P. Strohriegel, *Macromol. Chem. Phys.* 204 (2003) 1706.
- [50] G.W. Gray, M. Hird, D. Lacey, K.J. Toyne, *J. Chem. Soc., Perkin Trans. 2* (1989) 2041.
- [51] J. DePriest, G.Y. Zheng, N. Goswami, D.M. Eichhorn, C. Woods, D.P. Rillema, *Inorg. Chem.* 39 (2000) 1955.
- [52] J. DePriest, G.Y. Zheng, C. Woods, D.P. Rillema, N.A. Mikirova, M.E. Zandler, *Inorg. Chim. Acta* 264 (1997) 287.
- [53] M.M. Mdeleleni, J.S. Bridgewater, R.J. Watts, P.C. Ford, *Inorg. Chem.* 34 (1995) 2334.
- [54] M. Ghedini, D. Pucci, A. Crispini, G. Barberio, *Organometallics* 18 (1999) 2116.
- [55] J. Breu, K.J. Range, A.H. von Zelewsky, H. Yersin, *Acta Crystallogr. C* 53 (1997) 562.
- [56] T.J. Giordano, P.G. Rasmussen, *Inorg. Chem.* 14 (1975) 1628.
- [57] M. Maestri, D. Sandrini, V. Balzani, L. Chasson, P. Jolliet, A. von Zelewsky, *Chem. Phys. Lett.* 122 (1985) 375.
- [58] L. Chassot, A. von Zelewsky, *Inorg. Chem.* 26 (1987) 2814.
- [59] V.V. Grudhin, N. Herron, D.D. LeCloux, W.J. Marshall, V.A. Petrov, Y. Wang, *Chem. Commun.* (2001) 1494.
- [60] L. Sacksteder, A.P. Zipp, E.A. Brown, J. Streich, J.N. Demas, B.A. DeGraff, *Inorg. Chem.* 29 (1990) 4335.
- [61] V.W.W. Yam, R.P.L. Tang, K.M.C. Wong, K.K. Cheung, *Organometallics* 20 (2001) 4476.
- [62] A. Tsuboyama, H. Iwakaki, M. Furugori, T. Mukaide, J. Kamatani, S. Igawa, T. Moriyama, S. Miura, T. Takiguchi, S. Okada, M. Hoshino, K. Ueno, *J. Am. Chem. Soc.* 125 (2003) 12971.
- [63] M.S. Lowry, J.I. Goldsmith, J.D. Slinker, R. Rohl, R.A. Pascal Jr., G.G. Malliaras, S. Bernhard, *Chem. Mater.* 17 (2005) 5712.
- [64] M.S. Lowry, W.R. Hudson, R.A. Pascal Jr., S. Bernhard, *J. Am. Chem. Soc.* 126 (2004) 14129.
- [65] A.B. Tamayo, S. Garon, T. Sajoto, P.I. Djurovich, I.M. Tsyba, R. Bau, M.E. Thompson, *Inorg. Chem.* 44 (2005) 8723.
- [66] I.R. Laskar, T.M. Chen, *Chem. Mater.* 16 (2004) 111.
- [67] T. Suzuki, N. Shirasawa, T. Suzuki, S. Tokito, *Adv. Mater.* 15 (2003) 1455.
- [68] J.P. Duan, P.P. Sun, C.H. Cheng, *Adv. Mater.* 15 (2003) 224.
- [69] H.Z. Xie, M.W. Liu, O.Y. Wang, X.H. Zhang, C.S. Lee, L.S. Hung, S.T. Lee, P.F. Teng, H.L. Kwong, H. Zhen, C.M. Che, *Adv. Mater.* 13 (2001) 1245.
- [70] X.-M. Yu, G.-J. Zhou, C.-S. Lam, W.-Y. Wong, X.-L. Zhu, J.-X. Sun, M. Wong, H.-S. Kwok, *J. Organomet. Chem.* 693 (2008) 1518.
- [71] J. Pommerehne, H. Vestweber, W. Guss, R.F. Mahrt, H. Bässler, M. Porsch, J. Daub, *Adv. Mater.* 7 (1995) 551.
- [72] K.R.J. Thomas, J.T. Lin, Y.T. Tao, C.W. Ko, *J. Am. Chem. Soc.* 123 (2001) 9404.
- [73] Y. Hong, J. Kanicki, *IEEE Trans. Electron Dev.* 51 (2004) 1562.
- [74] R.C. Kwong, S. Lamansky, M.E. Thompson, *Adv. Mater.* 12 (2000) 1134.
- [75] J.-H. Li, S. Andresen, H.-H. Liao, Y. Yang, *ACS Appl. Mater. Interf.* 1 (2009) 76.
- [76] T.M. Brown, J.S. Kim, R.H. Friend, F. Cacialli, R. Daik, W.J. Feast, *Appl. Phys. Lett.* 75 (1999) 1679.
- [77] B.W. D'Andrade, M.A. Baldo, C. Adachi, J. Brooks, M.E. Thompson, S.R. Forrest, *Appl. Phys. Lett.* 79 (2001) 1045.
- [78] M.A. Baldo, M.E. Thompson, S.R. Forrest, *Nature* 403 (2000) 750.
- [79] C. Adachi, R.C. Kwong, P. Djurovich, V. Adamovich, M.A. Baldo, M.E. Thompson, S.R. Forrest, *Appl. Phys. Lett.* 79 (2001) 2082.
- [80] M.A. Baldo, S. Lamansky, P.E. Burrows, M.E. Thompson, S.R. Forrest, *Appl. Phys. Lett.* 75 (1999) 4.
- [81] C. Adachi, M.A. Baldo, S.R. Forrest, M.E. Thompson, *Appl. Phys. Lett.* 77 (2000) 904.
- [82] W. Lu, B.X. Mi, M.C.W. Chan, Z. Hui, N.Y. Zhu, S.T. Lee, C.M. Che, *Chem. Commun.* (2002) 206.
- [83] E.L. Williams, K. Haavisto, J. Li, G.E. Jabbour, *Adv. Mater.* 19 (2007) 197.
- [84] W. Lu, M.C.W. Chan, K.K. Cheung, C.M. Che, *Organometallics* 20 (2001) 2477.
- [85] W. Lu, B.X. Mi, M.C.W. Chan, Z. Hui, C.M. Che, N. Zhu, S.T. Lee, *J. Am. Chem. Soc.* 126 (2004) 4958.
- [86] C.M. Che, S.C. Chan, H.F. Xiang, M.C.W. Chan, Y. Liu, Y. Wang, *Chem. Commun.* (2004) 1484.
- [87] B.W. D'Andrade, J. Brooks, V. Adamovich, M.E. Thompson, S.R. Forrest, *Adv. Mater.* 14 (2002) 1032.
- [88] V. Adamovich, J. Brooks, A. Tamayo, A.M. Alexander, P.I. Djurovich, B.W. D'Andrade, C. Adachi, S.R. Forrest, M.E. Thompson, *New J. Chem.* 26 (2002) 1171.
- [89] J. Kalinowski, W. Stampor, J. Mezyk, M. Cocchi, D. Virgili, V. Fattori, P. Di Marco, *Phys. Rev. B: Condens. Mat. Mater. Phys.* 66 (2002) 235321.
- [90] G.-J. Zhou, W.-Y. Wong, B. Yao, Z.-Y. Xie, L.-X. Wang, *J. Mater. Chem.* 18 (2008) 1799.
- [91] Y. Wang, N. Herron, V.V. Grushin, D. LeCloux, V. Petrov, *Appl. Phys. Lett.* 79 (2001) 449.
- [92] Z. Bao, A.J. Lovinger, J. Brown, *J. Am. Chem. Soc.* 120 (1998) 207.
- [93] L.S. Hung, C.H. Chen, *Mater. Sci. Eng. R* 39 (2002) 143.
- [94] F. Babudri, G.M. Farinola, F. Naso, R. Ragni, *Chem. Commun.* (2007) 1003.
- [95] SAINT+, ver. 6.02a, Bruker, Analytical X-ray System, Inc., Madison, WI, 1998.
- [96] G.M. Sheldrick, SADABS, Empirical Absorption Correction Program, University of Göttingen, Germany, 1997.
- [97] G.M. Sheldrick, *SHELXTL™*, Reference Manual, ver. 5.1, Madison, WI, 1997.